Economic Geology, v. XXX, no. XX, pp. X–X

Genesis of the Questa Mo Porphyry Deposit and Nearby Polymetallic Mineralization, New Mexico, USA

Sean P. Gaynor,[1,2,†,] Joshua M. Rosera,[1,3] and Drew S. Coleman[1]*

[1] *Department of Earth, Marine and Environmental Sciences, University of North Carolina at Chapel Hill, Chapel Hill, North Carolina 27510, USA*

[2] *Department of Earth Sciences, University of Geneva, 13, Rue des Maraîchers, Geneva 1205, Switzerland*

[3] *U.S. Geological Survey, Geology, Energy & Minerals Science Center, Reston, Virginia 20192, USA*

Abstract

The Oligocene Latir magmatic center in northern New Mexico is an exceptionally well-exposed volcano-plutonic complex that hosts a variety of magmatic-hydrothermal deposits, ranging from relatively deep, F-rich porphyry Mo mineralization to shallower epithermal deposits. We present new whole-rock chemical and isotopic data for plutonic rocks from the Latir magmatic center, including extensive sampling of drill core samples of intrusive rocks from the Questa porphyry Mo deposit. These data document temporal chemical trends of porphyry-related mineralization that occurred after caldera-forming magmatism and during postcaldera batholith assembly. Silicic magmas were generated multiple times throughout the history of the Latir magmatic center, but few are associated with the formation of a mineral deposit. Whole-rock trace element ratios and Sr, Nd, and Pb isotope compositions vary throughout the protracted history of silicic magmatism. The caldera-forming ignimbrite and early phase of postcaldera intrusions are unmineralized, more enriched in high field strength elements, and generally contain less radiogenic Sr and Pb and more radiogenic Nd than later intrusions. The Questa porphyry Mo deposit formed immediately after the most isotopically primitive phase of the batholith was assembled, ruling out simple reworking of juvenile mantle-derived crust as the source for mineralizing magmas. Rhyolite dikes associated with polymetallic sulfide deposits intruded ~800 k.y. after Mo mineralization, and Nd isotope data indicate that these dikes are associated with different batches of magma and are unrelated to the Mo-mineralizing intrusions at the Questa mine. Together, these data indicate that the source of magmas changed significantly throughout the 10-m.y. history of the magmatic center. We assess multiple genetic models for porphyry-related magmatism against this data set, favoring models with discrete periods of magma genesis from a deep hybridized zone in the lower crust giving rise to the punctuated periods of mineralization. These observations suggest that the formation of mineral deposits within a central magmatic locus is likely the result of the piecemeal assembly of individual hydrothermal-magmatic systems, and that distal and younger polymetallic mineralization commonly observed near known porphyry deposits represents decoupled processes.

Introduction

Porphyry deposits host much of the world's Cu, Au, and Mo resources (e.g., high-sulfidation Au, polymetallic vein, and carbonate-replacement deposits; Hedenquist and Lowenstern, 1994; Heinrich et al., 2004; Sillitoe, 2010). Consequently, understanding porphyry ore systems—the suite of magmatic-hydrothermal mineral deposits that characterize porphyry and near-porphyry environments (e.g., Sillitoe, 2010)—is a significant topic of discussion and active research. A growing body of evidence demonstrates that upper crustal magma bodies are assembled incrementally by numerous small intrusions (e.g., Coleman et al., 2004; Michel et al., 2008; Gaynor et al., 2019b) rather than through long-lived, large, liquid-rich magma chambers (e.g., Miller and Paterson, 1999; Bachmann and Bergantz, 2004). This change in petrologic models for upper crustal magmas has subsequently forced a paradigm shift in the understanding of porphyry-style mineralization (e.g., Chelle-Michou et al., 2017; Korges et al., 2020). An important consequence of the incremental assembly hypothesis is that at any given time, the volume of melt in an upper crustal magma system is much smaller than the final observed volume of the assembled intrusion. Hence, chemical and physical models that require large, mostly liquid volumes of magma to explain porphyry mineralization events have become difficult to reconcile with a much more dynamic system in which the solid/melt ratio fluctuates through time.

Numerical modeling of variations in magma flux has improved our knowledge of how the probability of porphyry mineralization can be increased in upper crustal silicic magma systems. In particular, these studies lend insight into why individual mineralization events are typically short-lived (less than 10 k.y.) within much longer-lived upper crustal systems (5–10 m.y.; e.g., Chiaradia et al., 2013; Mercer et al., 2015a). Porphyry mineralization is favored when magma flux is lower than that associated with volcanic eruptions (~10^{-2} km^3/yr) but greater than that associated with barren plutonism (~10^{-4} km^3/yr; Caricchi et al., 2014; Chelle-Michou et al., 2017; Schöpa et al., 2017; Cox et al., 2020; Korges et al., 2020). This relationship occurs because volcanic eruptions are thought to be detrimental to subsequent mineralization due to destruction of existing deposits or preventing subsequent formation from the existing upper crustal magma system (e.g., Sillitoe, 1980; Pasteris, 1996). However, too low of a magma flux instead results in a low upward flux of magmatically derived fluids, and therefore decreased porphyry mineralization potential (e.g., Schöpa et al., 2017), but the decreased heat flow could favor shallow epithermal mineralization (Korges et al., 2020).

[†]Corresponding author: e-mail, sean.gaynor@princeton.edu

[*]Present address: Department of Geosciences, Guyot Hall, Princeton University, New Jersey 08544, USA.

ISSN 0361-0128; doi:10.5382/econgeo.5011; 21 p.
Digital appendices are available in the online Supplements section.

Submitted: June 22, 2022/Accepted: November 30, 2022

Another important variable not often accounted for in understanding porphyry mineralization is how each batch of magma might be generated from different source rocks through time, and therefore, transient high-flux episodes could correlate to melting of particularly fertile source rocks. For example, many models describing porphyry mineralization make simplifying assumptions that each new batch of magma has the same primitive composition (e.g., Chelle-Michou et al., 2017; Korges et al., 2020), or that variations in magma compositions are a function of a few components in the deep crust (e.g., depth of melting, melt reactions; Chiaradia et al., 2009, 2012; Chiaradia, 2015; Lee and Tang, 2020). However, long-lived magma systems can chemically modify the lower crust and lithospheric mantle (e.g., Johnson et al., 1990; Johnson, 1991; Farmer et al., 1991; Gonzales and Lake, 2016), and therefore the composition of deep crustal-derived intrusive batches may vary through time. Thus, models that attempt to characterize brief mineralization episodes in long-lived magma systems may need to also account for rapid temporal variations in magma sources.

The Latir magmatic center, exposed in north-central New Mexico, hosted significant F-rich porphyry Mo mineralization (the "Climax-type" Questa porphyry Mo deposit; Ludington and Plumlee, 2009), subeconomic Au, Ag, Cu, and Pb mineralization, and barren intrusions over a >10-m.y. magmatic history (Fig. 1). Thus, it presents an opportunity to test if magma source variations are correlated with porphyry-related mineralization. The Latir magmatic center has been well studied in order to better understand caldera and batholith evolution (e.g., Johnson and Lipman, 1988; Johnson et al., 1989, 1990). However, recent studies of the Questa porphyry Mo deposit indicate that the major Mo mineralization events were previously misattributed to exposures of large-volume intrusions rather than the amalgamated suite of smaller intrusions responsible for mineralization (Gaynor et al., 2019a). Here, we use a suite of subsurface and drill core samples from the Questa porphyry Mo deposit as well as silicic dikes associated with polymetallic vein prospects located elsewhere in the batholith to examine when and why mineralization occurred in respect to the evolution of the magma center. Previous studies have established detailed, high-precision geochronology for the region (Fig. 2; Table 1; Lipman et al., 1986; Tappa et al., 2011; Zimmerer and McIntosh, 2012; Rosera et al., 2013; Gaynor et al. 2019a, b) and allow us to evaluate when magma genesis may have shifted geochemically throughout the center, and if those shifts were associated with mineralization.

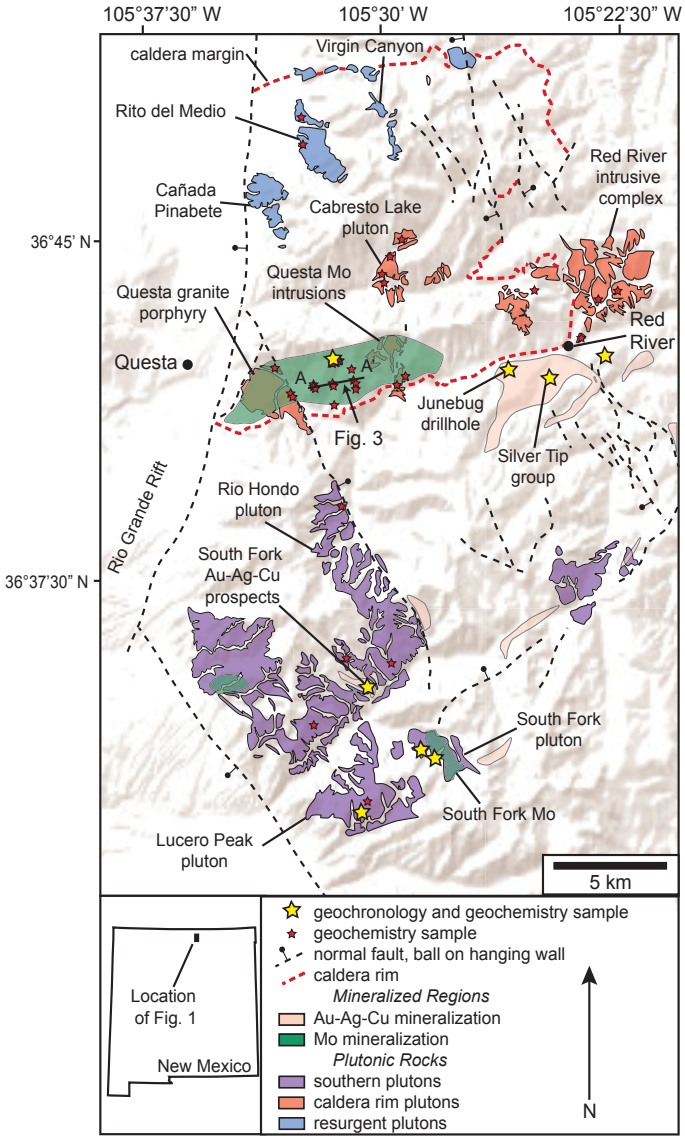

Fig. 1. Simplified geologic map of the Latir magmatic center, showing the sample locations for this study (modified from Lipman and Reed, 1989). Line A-A', due east of the town of Questa, is the location of Figure 3. The ball on hanging wall for some of the smaller normal faults has been omitted for clarity. Hillshade base modified from U.S. Geological Survey digital data.

Geologic Setting

Overview

The Latir magmatic center had a prolonged history of magmatism (>10 m.y.) that is preserved as volcanic (the Latir volcanic field) and plutonic (the Questa batholith) rocks punctuated by periods of magmatic-hydrothermal mineralization (Figs. 1, 2; Table 1; Lipman et al., 1986; Lipman and Reed, 1989; Tappa et al., 2011; Zimmerer and McIntosh, 2012; Rosera et al., 2013; Gaynor et al. 2019a, b). The volcanic-plutonic complex is exposed over approximately 1,200 km^2, and the regional sedimentary record suggests a substantial volume of volcanic rocks has been removed by erosion (Lipman et al., 1986; Smith et al., 2002). The volcanic field and batholith are truncated on the west side by the Rio Grande rift (Fig. 1). Extension began regionally at approximately 28 Ma, and the first igneous rocks preserved within the Latir magmatic center are 28.5 Ma andesites (Lipman et al., 1986; Olsen et al., 1987; Zimmerer and McIntosh, 2012; Ricketts et al., 2016). Oligocene-Miocene volcanism within the Latir magmatic center ranges in composition from andesite to rhyolite, including lavas and several small tuffs. These rocks are exposed within the northern portion of the Latir range, as well as within horst blocks within the rift (Thompson et al., 1986; Lipman and Reed, 1989; Zimmerer and McIntosh, 2012). A subvolcanic intrusive complex includes latite cut by porphyritic quartz latite dikes and sheets exposed along the Red River valley and represents the oldest intrusions known within the Latir mag-

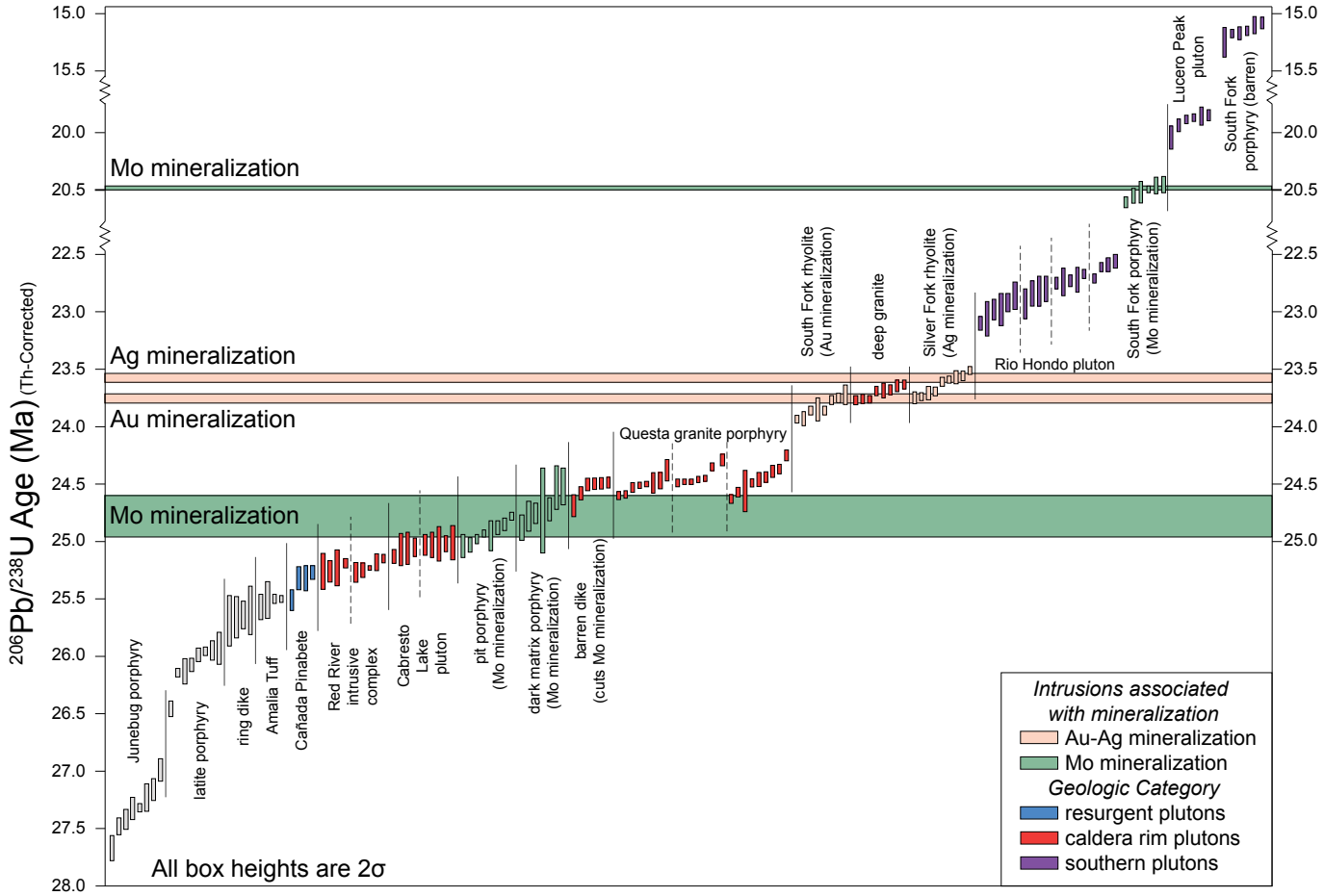

Fig. 2. Previously published chemical abrasion-isotope dilution-thermal ionization mass spectrometry (CA-ID-TIMS) U-Pb zircon geochronology data from the Latir magmatic center, highlighting the timing of crystallization of porphyry magmas associated with mineralization. The width of the bars associated with the timing of mineralization reflects either the weighted mean of the individual samples (e.g., South Fork Au; Silver Fork Ag) or the maximum possible duration for mineralization based on the weighted mean ages from igneous units that bracket mineralization (e.g., Questa porphyry Mo deposit). The y-axis omits two periods of magmatic lulls in the Latir magmatic center for clarity. Vertical lines separate individual rock samples; the lines are dashed where samples are from the same unit (e.g., Rio Hondo pluton) and solid when they represent different intrusive units. Data from Tappa et al. (2011), Rosera et al. (2013), Gaynor (2018), and Gaynor et al. (2019a and b).

matic center (Lipman and Reed, 1989; Meyer and Foland, 1991; Gaynor, 2018). Volcanism culminated with the eruption of the approximately 500-km^3 peralkaline Amalia Tuff at 25.52 Ma and subsequent collapse of the Questa caldera (Lipman et al., 1986; Tappa et al., 2011; Zimmerer and McIntosh, 2012).

Following the eruption of the Amalia Tuff, the majority of exposed plutonic rocks at Questa intruded over a period of at least 6.2 m.y., forming the Questa batholith (25.29–19.88 Ma; Fig. 2; Table 1; Tappa et al., 2011; Rosera et al., 2013; Gaynor et al., 2019a, b). Pluton assembly began immediately following the collapse of the Questa caldera, and exposed plutonic rocks become younger and structurally deeper toward the south owing to recent tilting associated with Rio Grande rifting and erosion (Snyder, 1984; Lipman et al., 1986; Hagstrum and Johnson, 1986; Meyer and Foland, 1991; Tappa et al., 2011; Gaynor et al., 2019b). On the basis of geographic location, age, and structural position within the magmatic center, the plutons are broadly grouped into three categories: resurgent plutons, caldera rim plutons, and southern plutons (Lipman et al., 1986).

Plutons

Resurgent plutons: The granitic resurgent plutons (Virgin Canyon; Cañada Pinabete, 25.3 Ma; Rito del Medio) are the northernmost intrusions and closest in age to the 25.52 Ma Amalia Tuff (Tappa et al., 2011; Zimmerer and McIntosh, 2012). Structurally higher phases of the Virgin Canyon and Cañada Pinabete plutons are peralkaline, whereas the structurally lower phases and the Rito del Medio are metaluminous (Johnson et al., 1989).

Caldera rim plutons: Caldera rim plutons (Red River Intrusive Suite, 25.20 Ma; Questa granite porphyry, 24.53–24.44 Ma) are exposed south of the resurgent plutons and are intermediate in age among exposed plutonic rocks (Meyer and Foland, 1991; Zimmerer and McIntosh, 2012; Rosera et al., 2013; Gaynor et al., 2019a, b). The Red River Intrusive Complex is a suite of fine-grained granodiorites cut by granite porphyries (Lipman and Reed, 1989). Although the Cabresto Lake pluton has previously been described as resurgent to the Questa caldera (Lipman et al., 1986), high-

Table 1. Relative and Absolute Chronology of the Latir Magmatic Center

Geologic unit	Age (Ma)[1]	Group	Mineral association	Reference
Barren South Fork dikes	15.269 ± 0.021	southern plutons	-	Gaynor et al., 2019b
Lucero Peak pluton	19.883 ± 0.017	southern plutons	-	Gaynor et al., 2019b
South Fork Mo-mineralizing dikes	20.494 ± 0.020	mineralization	Mo	Gaynor et al., 2019b
Rio Hondo pluton[2]	22.98 ± 0.09; 22.84 ± 0.06; 22.72 ± 0.05; 22.59 ± 0.06	southern plutons	-	Tappa et al., 2011
Ag-mineralizing dike	23.57 ± 0.02	mineralization	Ag	Gaynor et al., 2019b
Deep granite	23.67 ± 0.02	caldera rim plutons	-	Gaynor et al., 2019a
Au-mineralizing dike	23.77 ± 0.02	mineralization	Au	Gaynor et al., 2019b
Questa granite porphyry	24.53 ± 0.05; 24.46 ± 0.05; 24.44 ± 0.08	caldera rim plutons	Mo	Rosera et al., 2013
Postmineralization suite[3]	24.5 ± 0.02	caldera rim plutons	-	Gaynor et al., 2019a
Southwest porphyry[4]	-	mineralization	Mo	Gaynor et al., 2019a
Dark matrix porphyry	24.74 ± 0.048	mineralization	Mo	Gaynor et al., 2019a
Pit porphyry intrusion	24.91 ± 0.07	mineralization	Mo	Rosera et al., 2013
Northeast porphyry[4]	-	mineralization	Mo	Gaynor et al., 2019a
Central aplite[4]	-	mineralization	Mo	Gaynor et al., 2019a
Cabresto Lake pluton	25.09 ± 0.04; 25.02 ± 0.05	caldera rim plutons	-	Tappa et al., 2011
Red River intrusive complex	25.21 ± 0.06; 25.20 ± 0.04	caldera rim plutons	-	Rosera et al., 2013
Cañada Pinabete pluton	25.29 ± 0.05	resurgent plutons	-	Tappa et al., 2011
Amalia Tuff	25.52 ± 0.06		-	Tappa et al., 2011
Porphyritic quartz latite intrusion	26	precaldera rocks	-	Gaynor, 2018
Junebug porphyry	27.25	precaldera rocks	-	Gaynor, 2018
Pre-Amalia volcanic rocks	~29–27[5]	precaldera rocks	-	Zimmerer and McIntosh, 2012

[1]All dates are chemical abrasion-thermal ionization mass spectrometer (CA-TIMS) U-Pb zircon geochronology Th-corrected $^{206}Pb/^{238}U$ weighted mean ages unless otherwise noted; all uncertainties for these dates 2σ analytical uncertainties

[2]The Rio Hondo Pluton is a downward stacking pluton, with a protracted assembly

[3]Field relationships indicate the postmineral suite is a composite suite, both coeval with and postdating the Questa granite porphyry; samples collected for this study were selected to postdate the Questa granite porphyry based on crosscutting relationships, so the published geochronology does not reflect the samples used

[4]Absolute geochronology not available for some Mo-productive intrusive units; these units are organized by relative ages through cross cutting relationships (Gaynor et al., 2019a)

[5]Ar-Ar geochronology of biotite, hornblende, and sanidine

precision zircon geochronology indicates it intruded at approximately 25.1 Ma, or 100 k.y. after assembly of the Red River intrusive complex. Because of this, as well as its proximity to the intrusive complex at the Questa Mo mine, we herein consider the Cabresto Lake pluton as a caldera rim pluton even though it is not exposed near the caldera rim. The Questa granite porphyry includes units formerly mapped as the Bear Canyon and Sulphur Gulch plutons (Lipman and Reed, 1989), but more recently these have been interpreted to be the same unit on the basis of high-precision U/Pb zircon geochronology and structural analysis of drill hole data from the Questa porphyry Mo mine (Gaynor et al., 2019a). These plutons are also spatially and genetically associated with varying degrees of hydrothermal alteration and mineralization along the southern caldera margin, including fracture- and vein-hosted Cu-Au-Ag ± Mo mineralization and the F-rich Questa porphyry Mo deposit (McLemore and North, 1984; Livo and Clark, 2002; Ross et al., 2002). The small-volume intrusions associated with the Questa porphyry Mo deposit are discussed further below.

Southern plutons: The Rio Hondo pluton, which is the largest exposed intrusion in the Questa batholith, was assembled incrementally between 22.98 and 22.59 Ma (Tappa et al., 2011). It intruded after Au-Ag-Cu mineralization that occurred along the arcuate fracture system but before low-grade Mo mineralization in South Fork (20.49 Ma; Gaynor et al., 2019b). The Rio Hondo pluton was assembled from the top down, with older, high-silica granites above younger granodiorite. This temporal evolution is interpreted to reflect changes in magma genesis through time (Tappa et al., 2011). The 19.98 Ma Lucero Peak pluton intruded after assembly of the Rio Hondo pluton (Zimmerer and McIntosh, 2012; Gaynor et al., 2019b).

Questa porphyry Mo deposit

The Questa Mo deposit is a well-documented example of F-rich, porphyry-style mineralization resulting from episodic porphyritic intrusions and their magmatic-hydrothermal transition toward mineralizing fluids (e.g., Cline and Bodnar, 1994; Ross et al., 2002; Rowe, 2012; Rosera et al., 2013; Gaynor et al., 2019a). Detailed U-Pb zircon geochronology of intrusive rocks, Re/Os molybdenite geochronology from throughout the deposit, and three-dimensional structural reconstruction of the magmatic-hydrothermal complex demonstrate that the Questa Mo deposit was assembled incrementally by at least five crosscutting, discrete intrusive units between approximately 25.0 and 24.5 Ma (Figs. 2, 3; Gaynor et al., 2019a). From oldest to youngest, these intrusive units are the central aplite, northeast porphyry, pit porphyry, dark matrix porphyry, and southwest porphyry. Combined, they are approximately 0.62 km^3 (Gaynor et al., 2019a). The mineralizing intrusions have a limited range of mineralogical variation and a broad range of textural variation, including groundmass textures ranging from fine-grained to aplitic and sugary, and total phenocryst content ranging from nearly aphyric to just over 30 modal % (Gaynor et al., 2019a). These

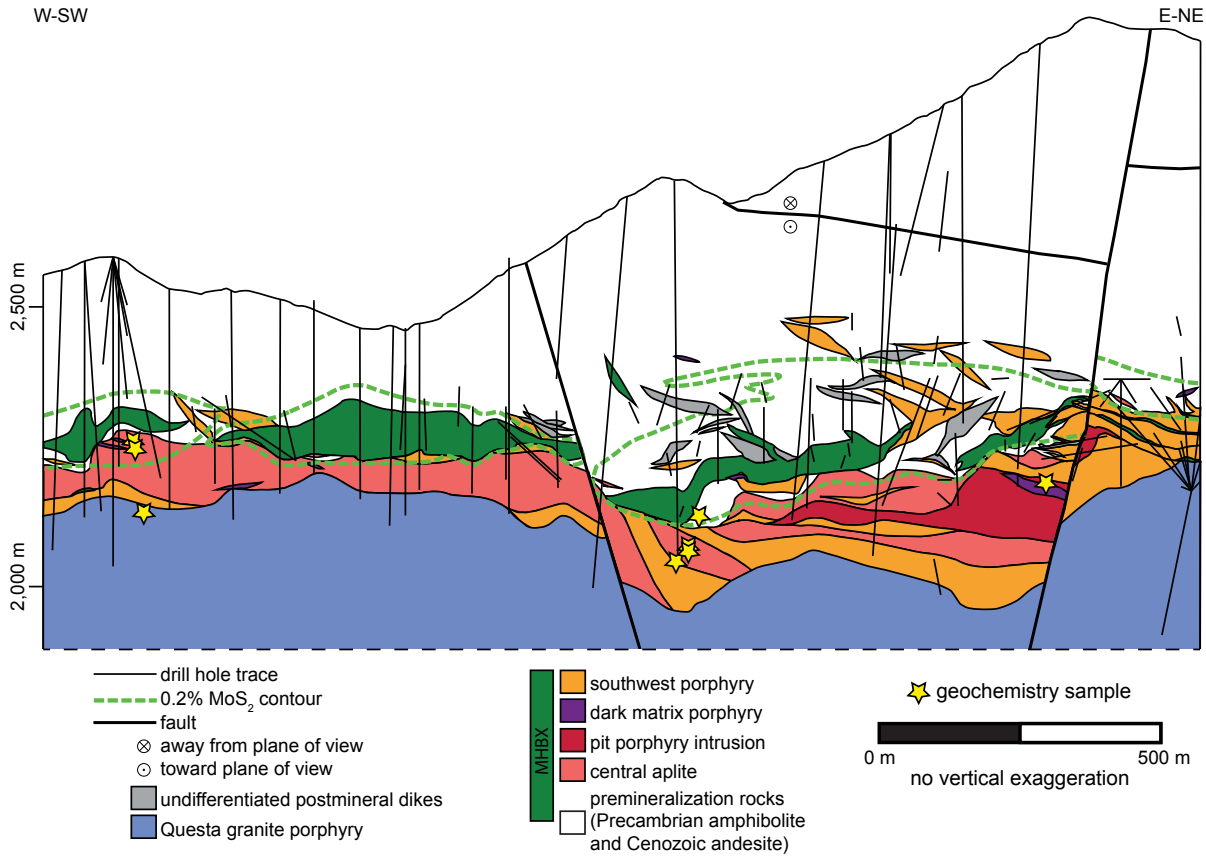

Fig. 3. Simplified geologic cross section from the Questa porphyry Mo deposit, highlighting the subeconomic Questa granite porphyry intrusion underlying a series of small-volume Mo-mineralizing intrusions. All subsurface sample locations shown on this figure are projected into section. Magmatic hydrothermal breccia (MHBX) bodies are commonly associated with high-grade ore, and in many cases have field relationships indicating multiple episodes of brecciation, alteration, and mineralization. The multiple episodes of MHBX formation and porphyry Mo mineralization at the Questa deposit were the result of punctuated magmatic-hydrothermal events during the protracted 400-k.y. formation of the deposit based on crosscutting relationships and high-precision U-Pb zircon geochronology (Gaynor et al., 2019a). Faults are shown as the bold, black lines. Drill core traces are only shown within a 60-m window of this section. The Questa granite porphyry extends deeper than the depth of this cross section and is underlain by the deep granite that was intercepted by drilling (not shown). No vertical exaggeration. Modified from Gaynor et al. (2019a).

intrusions are spatially, temporally, and genetically linked to high-grade zones of Mo mineralization (MoS_2 > 0.2 wt %) and relatively high-temperature alteration that typically transitions to lower-temperature assemblages away from the intrusive contacts. They intruded episodically until the intrusion of the Questa granite porphyry at 24.45 Ma (e.g., Ross et al., 2002; Rosera et al., 2013; Gaynor et al., 2019a). Their genetic relationship to Mo mineralization is based on crosscutting relationships, the orientation of mineralized veins emanating from intrusive roof contacts, unidirectional solidification textures underlying high-grade zones of Mo mineralization (e.g., Shannon et al., 1982; Carten et al., 1988), widespread aplitic textures (e.g., Carter et al., 2021), zonation of hydrothermal alteration away from intrusive contacts, the presence of narrow autobrecciated bands along intrusive contacts, spatial proximity to mineralization and potassic alteration, and coeval high-precision U-Pb zircon and Re-Os molybdenite geochronology (App. Table A1; Ross et al., 2002; Rosera et al., 2013; Gaynor et al., 2019a). Furthermore, based on those data, mineralizing intrusions at Questa rapidly intruded and mineralized their wall rock during discrete episodes during a broader assembly period of approximately 400 k.y. (Gaynor et al., 2019a).

The Questa granite porphyry underlies the deposit and is only associated with a relatively thin, discontinuous, low-grade (<0.05 wt % MoS_2) mineralization shell (Fig. 3; Rosera et al., 2013; Gaynor et al., 2019a). A suite of barren dikes along the caldera margin, ranging in composition from latite to rhyolite, postdate both the productive intrusions and the Questa granite porphyry (Gaynor et al., 2019a). One postmineral dike yielded a zircon U/Pb age coeval with the Questa granite porphyry at 24.5 Ma, indicating mineralization had waned by that time. Because the small-volume dikes and sheets associated with high-grade mineralization predate the large volume Questa granite porphyry, it is unlikely they have any genetic connection to high-grade mineralization (Gaynor et al., 2019a). An unmineralized, 23.67 Ma "deep granite" is not exposed at the surface and has only been intercepted underneath the Questa granite porphyry through exploratory drilling, but gravity modeling indicates that it likely underlies much of the southern caldera fault and Questa granite porphyry (Gaynor et al., 2019a, b).

Polymetallic sulfide mineralization

A suite of felsic dikes closely associated with polymetallic Au, Ag, Cu, Mo, Pb, and Zn vein- and shear-hosted mineralization intruded an arcuate fault system which extended from the town of Red River in an approximately south to southwest direction into the Rio Hondo drainage (Fig. 1; Schilling, 1960; Ludington et al., 1983; Jones, 1990). The intrusive contacts of some of the silicic dikes are pervasively altered and were targets of historical mining. Southwest of the town of Red River, along Pioneer Creek, a group of mines and prospects referred to as the Silver Tip Group (Fig. 1) coincide with silicified and argillized intrusions and breccias that contained auriferous pyrite as well as chalcopyrite and malachite (Schilling, 1960). Rock chip surveys in Pioneer Creek yielded anomalously high abundances of Ag in some places (>1 oz/ton; Ludington et al., 1983). Exploratory drilling in the Junebug hydrothermal scar intercepted similar rhyolite porphyries and alteration patterns near the base of the volcanic rocks and within Precambrian granite. Rhyolite dikes in the Junebug drill core contain haloes of quartz-sericite veins with potassic selvages, and surrounding wall rocks contain 0.5 to 3.0 modal % pyrite.

In the South Fork drainage, relatively unaltered crosscutting silicic dikes have intensely altered and silicified wall rocks, and these alteration zones are mineralized with low-grade Au, Ag, and Cu (Schilling, 1960; Ludington et al., 1983). The spatial association of the dikes and mineralization has been interpreted to be evidence of a genetic link between the two. Silicic dikes spatially associated with Au-Ag-Cu mineralization yielded ages similar to the deep granite (South Fork dike: 23.77 Ma; Silver Tip Group dike: 23.57 Ma; Gaynor et al., 2019b). To the south of the South Fork Au-Ag-Cu prospects, silicic dikes and subparallel fractures cut the South Fork pluton and host quartz-molybdenite veins (Fig. 1; Jones, 1990). The Mo-mineralizing dikes near South Fork yielded a zircon age of 20.49 Ma (Gaynor et al., 2019b). Thus, Au-Ag-Cu-Mo mineralization associated with the arcuate dike swarm occurred episodically over approximately 3 m.y.. A younger suite of 15.3 Ma unmineralized dikes cuts the arcuate swarm and trends northwest-southeast, subparallel to range-bounding normal faults (Zimmerer and McIntosh, 2012; Gaynor et al., 2019b). This swarm of dikes is not associated with any historical mining or prospects (Jones, 1990).

Methods

To assess the temporal evolution of the Latir magmatic center, geologic units were organized by relative and absolute age relationships and published relationships between intrusive units and mineralization (Table 1; App. Table A1). Samples from the Latir magmatic center were collected from surface outcrops as well as underground exposures and drill core from the Questa mine and surrounding region, including samples characterized in previous studies (App. Table A2; e.g., Zimmerer and McIntosh, 2012; Gaynor et al., 2019a, b). Care was taken to ensure samples picked for geochemical characterization had no vein material and had not undergone alteration, identified through the presence of disseminated minerals such as pyrite, sericite, or calcite. This could not be fully avoided for some of the older intrusions that only occur in the altered zones of the Questa porphyry Mo deposit, as well as for samples from the South Fork Au prospect and Silver Tip and Junebug prospects. To aid in assessing the effects of alteration, we calculated an alteration index (AI; Ishikawa et al., 1976; Mathieu, 2018) for each sample. The AI values are between 0 and 100, and generally unaltered felsic rocks have AI below ~70, whereas altered samples have higher AI. Detailed sample descriptions can be found in Appendix Table A1.

Major and trace element geochemistry

Samples were crushed with a jaw crusher to centimeter-sized chips, then powdered in an alumina-ceramic shatterbox. Chemical analyses were completed by ActLabs (Ontario, Canada) and at the University of North Carolina at Chapel Hill. Samples analyzed by ActLabs were dissolved by fusion in a lithium metaborate/tetraborate mixture; major elements and Ba, Sr, Y, Zr, Sc, Be, and V were analyzed by inductively coupled plasma-optical emission spectroscopy (ICP-OES), and remaining trace elements and rare earth elements (REEs) were analyzed by inductively coupled plasma-mass spectrometry (ICP-MS). Uncertainties ($\pm 2\sigma$ relative) for major elements analyzed at ActLabs were less than 2% for all oxides except MgO (3%), MnO (5%), and P_2O_5 (16%), based on replicate measurements of U.S. Geological Survey standards. Trace elements determined at ActLabs that are reproducible at better than 2 ppm ($\pm 2\sigma$ absolute) include Ag, Be, Cs, Ge, Hf, Sb, Sn, Ta, Th, Tl, U, and W. Other elements are reproducible within 3 ppm (Co, Mo, Nb, Sc) and 4 ppm (Ga, Y), and others have higher uncertainties, in parentheses in ppm: Pb (9); Cu (14); Rb and Zr (15); V (19); Ni (23); Sr (25); Ba (31); Zn (42); Cr (49). REEs reproducible ($\pm 2\sigma$ absolute) at 0.2 ppm or better are Eu, Ho, Lu, Tb, and Tm; REEs reproducible at 0.2 to 0.5 ppm or better are Dy, Er, Gd, Pr, Sm, and Yb; others are reproducible at higher uncertainties, in ppm: Nd (1.2); La (1.5); Ce (2.1). Detection limits can be found in Appendix Table A3.

At the University of North Carolina at Chapel Hill, samples were prepared as fused discs for major element determinations and pressed powder pellets for trace element determinations using a Rigaku Supermini wavelength-dispersive X-ray fluorescence (XRF) spectrometer. Fused discs were prepared following procedures in Putnam et al. (2015). For trace element analysis, unignited samples (10 g) were mixed with 4 g of an Elvacite-acetone solution (250 g/1 L) and left for two hours to evaporate the acetone. Dried mixtures were mixed and disaggregated with a mortar and pestle prior to being hydraulically pressed into an aluminum mold. Calibrations for both major and trace elements were run against standards AGV-1, G-2, QLO-1, RGM-1, GSP-2, NST 278, MAG-1, BHVO-1, and DNC-1 (e.g., Jochum et al., 2015). Analytical errors for these samples were determined by analyzing AGV-2 and GSP-2 standard samples as unknowns.

Isotope geochemistry

Roughly 10 to 200 mg of whole-rock powder was dissolved in HF and HNO_3 in Teflon (Parr) bombs at approximately 180°C for 48 to 72 hours. Samples were dried down to purge Si, and then immediately fluxed in concentrated HCl for 8 to 16 hours. Samples were aliquoted for isotope chemistry on the basis of estimated or previously determined elemental

concentrations. Strontium was purified using Sr-spec cation exchange resin using the methods of Lundblad (1994) and loaded on single Re filaments with a TaF_5 activator to enhance ionization. Neodymium and Sm were purified through a three-stage column chemistry procedure following Harvey and Baxter (2009). Only Nd was eluted for samples for which [Sm] and [Nd] were determined by ActLabs. Remaining samples were spiked with a mixed ^{150}Nd-^{149}Sm tracer solution. Lead was purified using anion exchange column chemistry using an HBr chemistry technique modified after Parrish et al. (1987) and loaded on single Re filaments with H_3PO_4 and silica gel (Cameron et al., 1969). Total procedural blanks were less than 0.1 ng for Sr, 0.2 ng for Nd, and 0.1 ng for Pb. Whole-rock Sr, Sm, and Pb isotope compositions were determined on a VG Sector 54 thermal ionization mass spectrometer (TIMS) at the University of North Carolina at Chapel Hill using Faraday detectors (10^{11} Ω resistors). Strontium isotope compositions were determined as a metal in dynamic-multicollector mode with ^{88}Sr = 3V. Strontium isotope ratios were corrected for mass fractionation using an exponential law correction and normalized to $^{86}Sr/^{88}Sr = 0.1194$. Replicate analyses of the NBS 987 Sr standard yielded $^{87}Sr/^{86}Sr = 0.710265 \pm 15$ (2σ, n = 26). Samarium was determined as a metal in static-multicollector mode. Lead isotope compositions were determined in static-multicollector mode with ^{208}Pb = 2V. Lead isotope ratios were corrected for mass fractionation by 0.12% per a.m.u. as determined by replicate analyses of NBS 981 (n = 17). Neodymium isotope compositions were determined on an IsotopX Phoenix-X62 TIMS at the University of North Carolina at Chapel Hill using Faraday detectors (10^{11} Ω resistors). Neodymium isotope compositions were determined as an oxide in dynamic-multicollector mode with $^{142}Nd^{16}O$ = 1V. Neodymium isotope compositions were normalized to $^{146}Nd/^{144}Nd = 0.7219$ and referenced to $^{143}Nd/^{144}Nd = 0.512102 \pm 8$ (JNdi, n = 114). Epsilon values were calculated using a modern chondritic uniform reservoir (CHUR) value of $^{143}Nd/^{144}Nd = 0.512638$ and $^{147}Sm/^{144}Nd = 0.1967$. All isotope ratios were corrected to initial values using elemental data obtained from ActLabs and crystallization ages obtained by ID-TIMS U/Pb zircon analyses or interpolated ages between dated intrusions, and using decay constants of $\lambda^{87}Rb = 1.42 \times 10^{-11}$ a^{-1}, $\lambda\ ^{147}Sm = 6.54 \times 10^{-12}$ a^{-1}, $^{235}U = 9.85 \times 10^{-10}$ a^{-1}, and $^{238}U = 1.55 \times 10^{-11}$ a^{-1} (Davis et al., 1977; Jaffey et al., 1971; Lugmair and Marti, 1978; Table 1).

Results

Precaldera rocks, Amalia Tuff, and early plutons

Thirteen samples of rocks that predate major Mo mineralization (>25 Ma) in batholith were analyzed from the resurgent plutons and early caldera rim plutons. These include samples from precaldera shallow quartz latite and quartz latite porphyry intrusions, the Amalia Tuff, the Rito del Medio pluton, the Red River intrusive complex, and the Cabresto Lake pluton. Pre-Mo–mineralization magmas are intermediate to silicic (SiO_2 = 63–79 wt %; Figs. 4, 5). This group of samples did not show any significant textural or mineralogical evidence for alteration, and their AI is below 60 (App. Table A1; Fig. A1). The pre-Mo–mineralization magmas have large variations in trace element values through time (Fig. 6). The two precaldera samples analyzed have relatively low Zr, Nb, and Y abundances, and similarly low Rb/Sr and high Sr/Y ratios (Fig. 5). The Amalia Tuff and early resurgent plutons within the caldera (e.g., the Rito del Medio pluton), however, are characterized by high concentrations of high-field strength elements (HFSEs) Zr, Nb, and Y, and correspondingly high Rb/Sr and low Sr/Y ratios. A 25.2 Ma granodiorite from the Red River intrusive suite (Rosera et al., 2013) yielded HFSE abundances and trace element ratios comparable to the precaldera rocks (Fig. 5).

One sample of the Amalia Tuff yields $^{87}Sr/^{86}Sr_i = 0.71306$ and $\varepsilon_{Nd}(t) = -5.99$. The precaldera quartz latite intrusions and earliest resurgent pluton analyzed (Rito del Medio; Fig. 1; App. Tables A4 and A5) have $^{87}Sr/^{86}Sr_i$ between 0.7051 and 0.7217 and $\varepsilon_{Nd}(t)$ between –4.98 and –6.47 (Figs. 7, 8). The younger Red River intrusive suite and Cabresto Lake pluton have variable isotopic compositions, but overall have less radiogenic Sr and more radiogenic Nd isotope compositions than the preceding intrusions ($^{87}Sr/^{86}Sr_i$ = 0.70387–0.7074; $\varepsilon_{Nd}(t)$ = –4.34 to –6.81). Within the Red River intrusive complex and Cabresto Lake pluton, initial $^{206}Pb/^{204}Pb$ ranges from 17.67 to 18.16 and $^{208}Pb/^{204}Pb$ ranges from 37.22 to 37.45 (Fig. 9; App. Table A9). Lead isotopes were analyzed from one precaldera quartz latite, yielding $^{206}Pb/^{204}Pb_i = 17.67$ and $^{208}Pb/^{204}Pb_i = 37.34$.

Intrusions from the Questa porphyry Mo deposit

Mo-mineralizing intrusions: Ten samples from the five Mo-mineralizing intrusive units from the Questa porphyry Mo deposit were analyzed for this study (in relative age order: central aplite/northeast porphyry, dark matrix porphyry, pit porphyry intrusion, southwest porphyry; Table 1; App. Table A1; Gaynor et al., 2019a). Overall, these mineralizing intrusions are characterized by low MgO (<1 wt %) and high SiO_2 (69–80 wt %), K_2O (4–8 wt %), and Rb (>150 ppm; Figs. 4, 5). Whereas almost all units associated with mineralization have major element compositions similar to high-silica rhyolites, the dark matrix porphyry has a dacitic composition. All of these intrusions have intermediate HFSE abundances when compared to pre- and postmineralizing intrusions in the Latir (Figs. 5, 6). Whereas Y and Sr are negatively correlated with SiO_2, Nb does not vary significantly.

The Sr, Nd, and Pb isotope ratios of Mo-mineralizing intrusions are intermediate relative to preceding intrusions (Red River Intrusive Suite and Cabresto Lake) and the postdating Questa granite porphyry ($^{87}Sr/^{86}Sr_i$ = 0.7051–0.7067; $\varepsilon_{Nd}(t)$ = –4.28 to –5.66; $^{206}Pb/^{204}Pb$ = 17.88–18.02, $^{207}Pb/^{204}Pb$ = 15.52–15.55, and $^{208}Pb/^{204}Pb$ = 37.25–37.36; Figs. 7–9). Five samples from this group have AI >70, consistent with observations of trace disseminated sericite. The entire mass of the central aplite is affected to some degree by early potassic flooding, as is evidenced by its high K_2O and AI values. Despite the presence of some alteration in many of the small mineralization intrusions from the Questa Mo deposit, there is no obvious correlation between alteration and isotopic compositions (App. Fig. A1)

Late-stage granites and dikes: Assembly of the Questa porphyry Mo deposit was followed by intrusion of weakly mineralized to unmineralized plutons and dikes (Figs. 1, 3). We

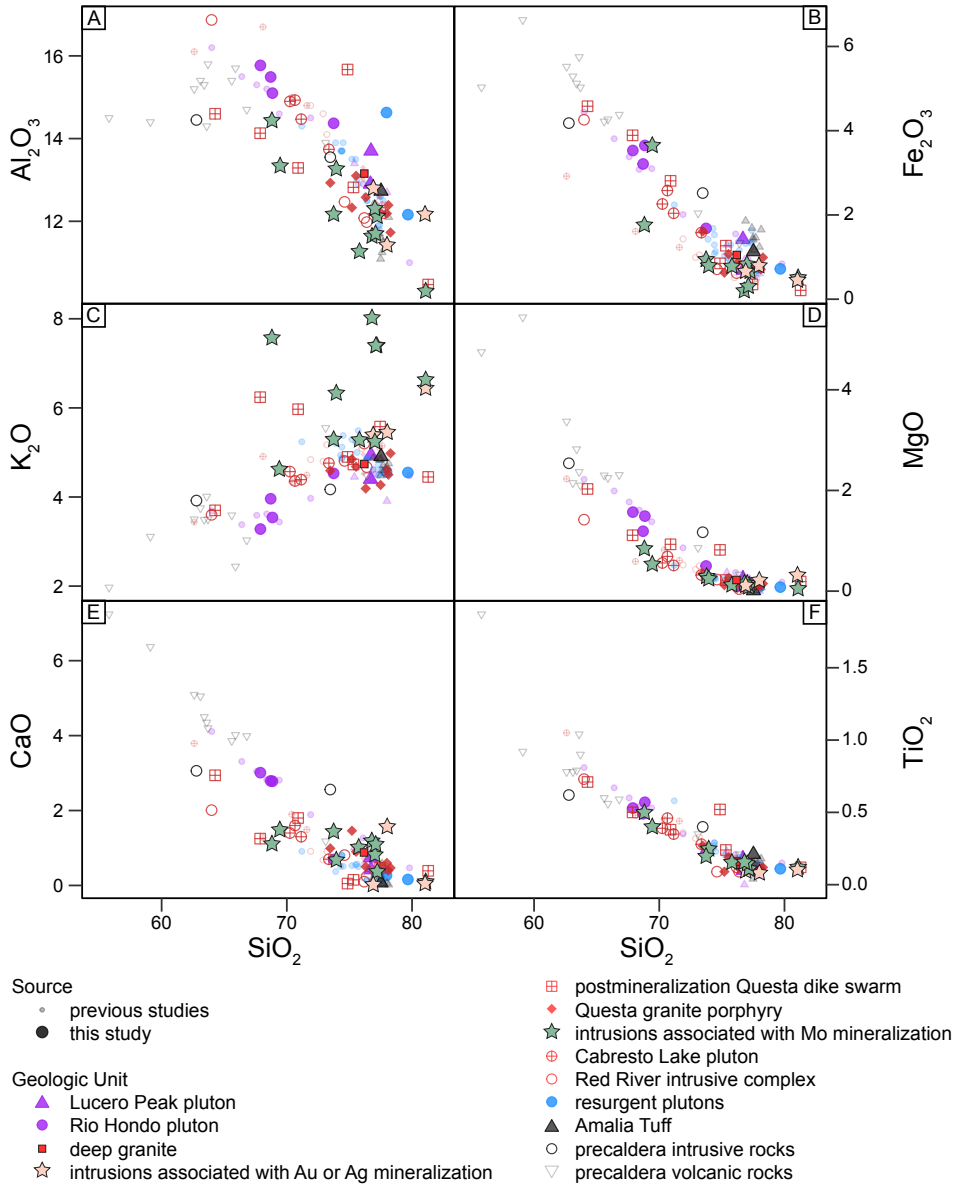

Fig. 4. Major element variation Harker diagrams for the rocks from the Latir magmatic center. Includes data from Johnson and Lipman (1988) and Johnson et al. (1989). All data are plotted as wt % oxide. Major element trends are largely independent of temporal groups. Note that all previously published data are shown in a smaller symbol size than the new data presented here.

analyzed 16 samples from this group of rocks (including the Questa granite porphyry, post-Mo–mineralization dikes, and the deep granite). Postmineralization dikes crosscut both the high-grade Mo mineralization and the Questa granite porphyry (Gaynor et al., 2019a). These intrusions range from intermediate to felsic (SiO_2 = 64–81 wt %; Fig. 4). Some of the dikes collected near the Questa Mo mine site were altered to quartz-sericite assemblage, resulting in moderate bleaching and alteration indices >70 for some of the samples (App. Table A1; Fig. A1). The Questa granite porphyry and postmineralization dikes have trace element compositions similar to the pre-Mo–mineralization caldera margin intrusions (e.g., Sr/Y = 1.0–50; Rb/Sr = 0.2–8.4; Fig. 5). The Questa granite porphyry is the most isotopically heterogeneous of any plutons within the field ($^{87}Sr/^{86}Sr_i$ = 0.7042–0.7066; $\varepsilon_{Nd}(t)$ = –5.88 to –7.54; $^{206}Pb/^{204}Pb$ = 17.87–18.09, $^{207}Pb/^{204}Pb$ = 15.51–15.54, $^{208}Pb/^{204}Pb$ = 37.19–37.33; Figs. 7–9). The postmineralization dike suite has less compositional variety in its isotopes, with less radiogenic Sr and Pb and more radiogenic Nd compositions ($^{87}Sr/^{86}Sr_i$ = 0.7035–0.7057; $\varepsilon_{Nd}(t)$ = –4.81 to –6.02; $^{206}Pb/^{204}Pb$ = 17.40–18.05; $^{207}Pb/^{204}Pb$ = 15.47–15.53; $^{208}Pb/^{204}Pb$ = 37.07–37.31; Figs. 7–9). The lowest $^{87}Sr/^{86}Sr_i$ corresponds to the most altered sample we analyzed (sample RD-13-18), which also has the lowest Sr/Y. However, the $\varepsilon_{Nd}(t)$ for this sample is comparable to other post-Mo dikes we analyzed (App. Fig. A1).

Dikes associated with polymetallic mineralization

Three silicic dikes closely associated with low-grade polymetallic mineralization, which extend from the town of

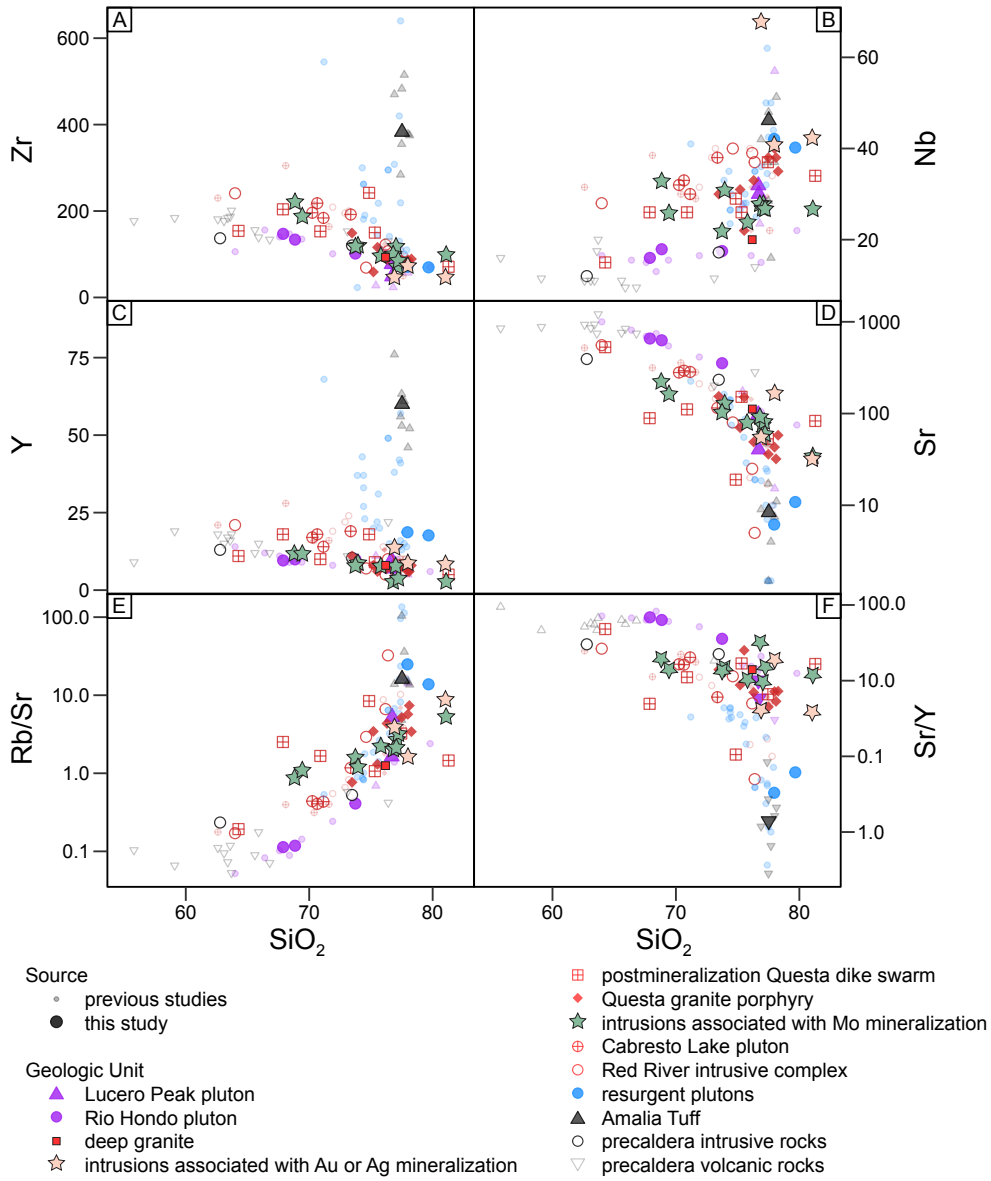

Fig. 5. Trace element variation Harker diagrams for the rocks from the Latir magmatic center. Includes data from Thompson et al. (1986), Johnson and Lipman (1988), and Johnson et al. (1989). Y-axes are in ppm. Y-axes for Sr, Rb/Sr, and Sr/Y are presented in logarithmic scale. X-axes are in wt %. Note that all previously published data are shown in a smaller symbol class than the new data presented here.

Red River toward South Fork (Fig. 1), were analyzed. The dikes are highly silicic (77–81 wt % SiO_2) and enriched in K_2O (5.5–6.5 wt %; Fig. 4). The silicic dike associated with mineralization at the Silver Tip mine hosts disseminated quartz-sericite alteration and has an AI near 100. This sample has similar Nd isotope compositions to a rhyolite dike intercepted in the Junebug exploration hole (both approximately $\varepsilon_{Nd}(t)$ = –6.6), but distinct initial Sr compositions ($^{87}Sr/^{86}Sr_i$ = 0.7025–0.7057). The silicic dike associated with Cu-Au-Ag mineralization near South Fork has distinct Sr and Nd isotope compositions ($^{87}Sr/^{86}Sr_i$ = 0.7043; $\varepsilon_{Nd}(t)$ = –5.51), which differ from the Silver Tip and Junebug silicic dikes. One sample from this group, the Junebug rhyolite, gave a $^{206}Pb/^{204}Pb_i$ value of 17.950 and a $^{208}Pb/^{204}Pb_i$ value of 37.217.

Southern plutons and Miocene dikes

Seven samples of the Rio Hondo pluton, the Lucero Peak pluton, and a 15.3 Ma unmineralized dike cutting the South Fork pluton were analyzed. The Rio Hondo pluton ranges from 68 to 73 wt % SiO_2 and contains lower Zr, Nb, and Y abundances and higher Sr concentrations than the earlier plutons and dikes (Figs. 4–6). The ratio of Rb/Sr is lower and Sr/Y is higher in the Rio Hondo than in older intrusions (Figs. 5, 6). Two samples from the Lucero Peak pluton are more silicic than the Rio Hondo pluton (~77 wt % SiO_2) and have trace element abundances and ratios comparable to granites from the Questa porphyry Mo deposit. The Rio Hondo and Lucero Peak plutons have nonradiogenic isotope compositions compared to preceding magmatism within the Latir magmatic

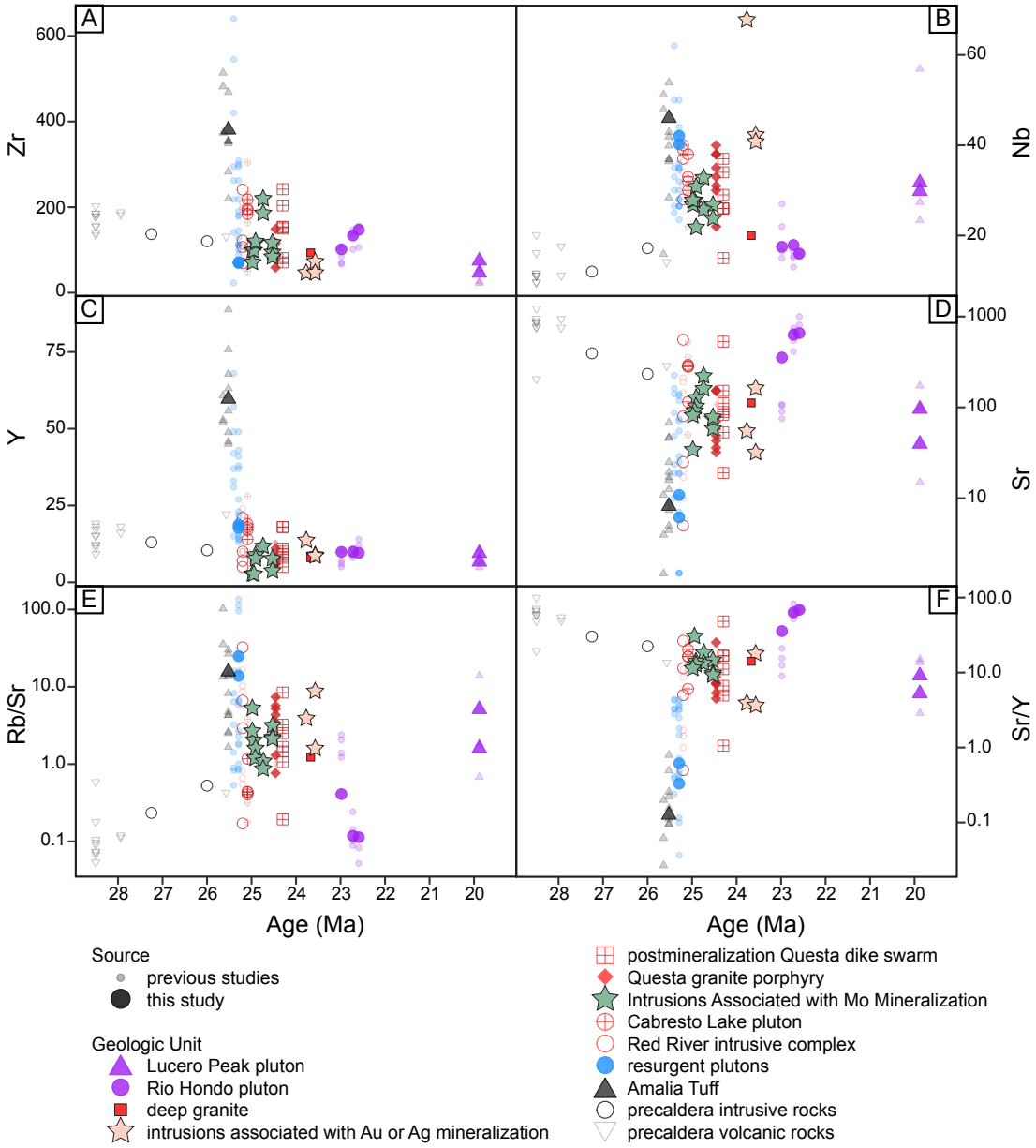

Fig. 6. Trace element geochemistry for rocks from the Latir magmatic center through time, showing that, whereas individual magmatic pulses may be geochemically distinct, there is not a specific geochemical signature related with mineralizing or barren intrusions. Includes data from Thompson et al. (1986), Johnson and Lipman (1988), and Johnson et al. (1989). Y-axes are in ppm. Y-axes for Sr, Rb/Sr, and Sr/Y are presented in logarithmic scale. Ages from Table 1. Note that all previously published data are shown in a smaller symbol class than the new data presented here.

center ($^{87}Sr/^{86}Sr_i$ = 0.7046–0.7052; $\varepsilon_{Nd}(t)$ = –6.25 to –6.72; Figs. 7, 8). The late, barren dike cutting the South Fork pluton has a very radiogenic Sr and nonradiogenic Nd composition relative to other southern pluton samples analyzed in this study ($^{87}Sr/^{86}Sr_i$ = 0.7088; $\varepsilon_{Nd}(t)$ = –7.07). These samples show no significant evidence of alteration (App. Table A1).

Discussion

Combining new geochemical data with existing geochemistry and geochronology of the Latir magmatic center reveals a complicated magmatic history characterized by porphyry-style mineralization, pre- and intermineralization pluton assembly, and batholith construction. These data allow for a reexamination of models of potential relationships between batholith formation and mineralization and the associations of different metals in porphyry systems.

Effects of hydrothermal alteration on whole-rock analyses

Although sampling methods targeted unaltered rocks, some samples were clearly affected by subsolidus alteration. A few samples collected from intrusions associated with high-grade Mo orebodies in the Questa porphyry Mo deposit have unusually high K_2O concentrations (Fig. 4), K_2O/Na_2O >2.5, and alteration indices >70, which are greater than what is generally considered unaltered felsic rock (Mathieu, 2018). The Mo-mineralizing intrusions at Questa occupy only a small vol-

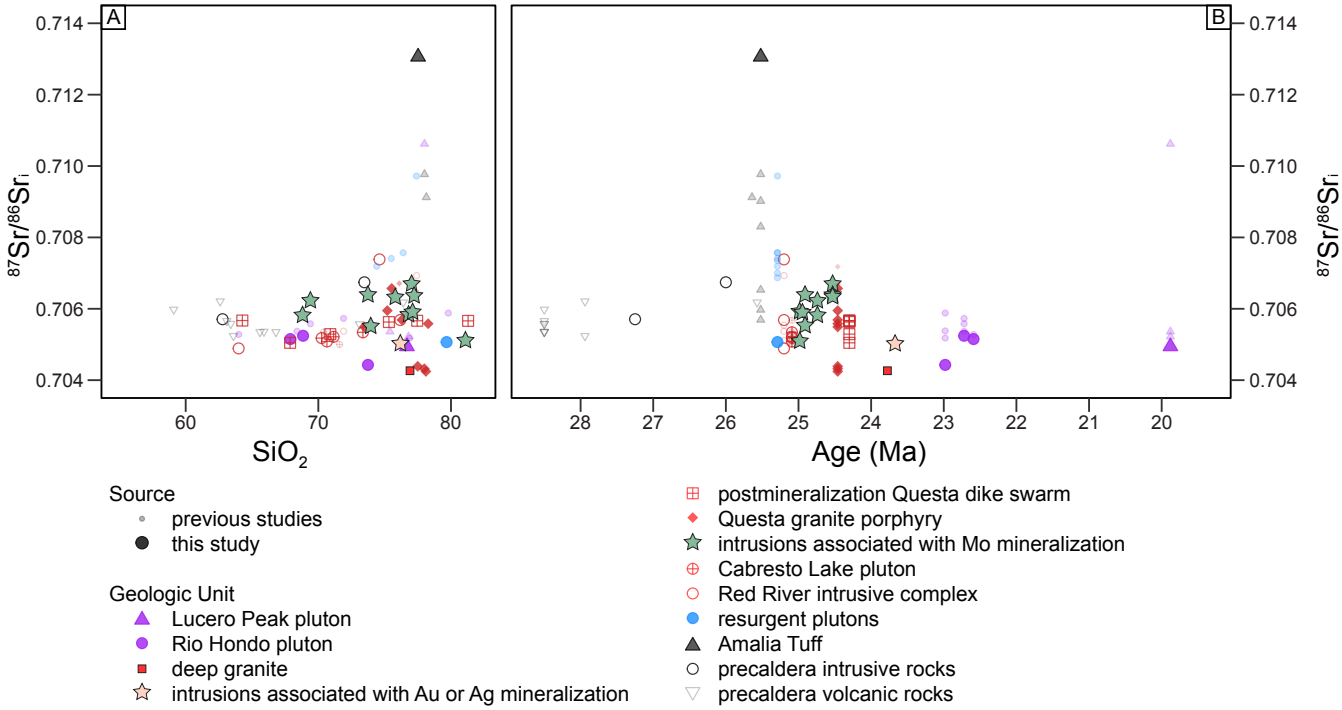

Fig. 7. Initial Sr isotope compositions of igneous rocks from the Latir magmatic center throughout its evolution, relative to SiO_2 composition (wt %; A) and relative to time (B). Includes data from Thompson et al. (1986) and Johnson et al. (1990). Ages from Table 1. Note that all previously published data are shown in a smaller symbol class than the new data presented here.

ume of the total deposit (~0.62 km^3 out of >15 km^3; Gaynor et al., 2019a), of which nearly the entire volume of rock has been affected by some degree of alteration. The HFSEs and REEs are more resistant to hydrothermal alteration (e.g., Farmer and DePaolo, 1984), and therefore are one of the main tools used in this study. Although other studies have demonstrated that significant alteration can modify $^{147}Sm/^{143}Nd$ ratios (e.g., Li et al., 2018), it commonly takes significantly more time than has elapsed since the Oligocene formation of the batholith and its deposits to allow for radiogenic ingrowth to alter the $^{143}Nd/^{144}Nd$ composition from equilibrium with its initial composition (e.g., Thompson et al., 2008). Furthermore, there is no correlation between AI and Sm/Nd or $\varepsilon_{Nd}(t)$ for the Mo mineralizing suite (App. Fig. A1). Therefore, we consider HFSEs and REEs, as well as the Nd isotope compositions, as largely representing unaltered equivalents of the igneous rocks in this study (e.g., Farmer and DePaolo, 1984). Lead isotope systematics appear to be largely unaffected in the altered samples; U and Th are not correlated with high AI, and the Pb isotope composition of high-AI samples does not significantly vary compared to less-altered rocks in the Questa deposit.

A small subset of samples from the Questa mine have geochemical compositions significantly affected by alteration. For example, two samples with both silicic and potassic alteration yield AI values >90 and have $^{87}Sr/^{86}Sr$ values that are lower than fresh or moderately altered samples (App. Fig. A1). This is potentially due to overcorrections for radiogenic Sr in-growth for samples where K (and Rb) was externally introduced during alteration. Consequently, two samples have age-corrected $^{87}Sr/^{86}Sr$ values that are unusually low (e.g., 0.7035 in a silicic dike). We have removed these samples from Figure 7 and do not include them in the following discussion.

Geochemical evolution of the Latir magmatic center

The newly established geochronological framework and access to subsurface samples reveal geochemical variability at multiple temporal (and spatial) scales in the Latir magma center. At the relatively short time scales of individual intrusive units there is moderate isotopic variation. For example, the Questa granite porphyry was assembled rapidly at approximately 24.5 Ma (Gaynor et al., 2019a), but has a relatively large range of $\varepsilon_{Nd}(t)$ from –7.25 to –5.15 (Fig. 8; App. Table A5). However, individual intrusive pulses in the Questa batholith typically have little overlap in ε_{Nd} with the intrusions that immediately precede and postdate them.

In order to discern larger-scale variations, we group isotopic and trace element variations into distinct trends highlighted in the violin plot in Figure 10 (Trends I and II). Trend I, from approximately 25.5 to 24.9 Ma, is characterized by silicic plutons that intruded the caldera before Mo mineralization and corresponds to increasing $\varepsilon_{Nd}(t)$ and Sr/Y through time (Fig. 10). During Trend I, initial $^{87}Sr/^{86}Sr$ and $^{206}Pb/^{204}Pb$ ratios become less radiogenic (Figs. 7, 9), and Y and Zr concentrations broadly decrease through time (Fig. 6). Trend II is defined by a reversal of these geochemical trends at the onset of Mo mineralization at Questa at approximately 25.0 Ma and continue along that trajectory until approximately 23.8 Ma with the intrusion of the deep granite and rhyolite dikes along the southern caldera margin. During Trend II, Sr/Y of magmas decreases slightly (Fig. 10), whereas $\varepsilon_{Nd}(t)$ tends to be more variable, but broadly decreases through time. Initially, $\varepsilon_{Nd}(t)$ declines

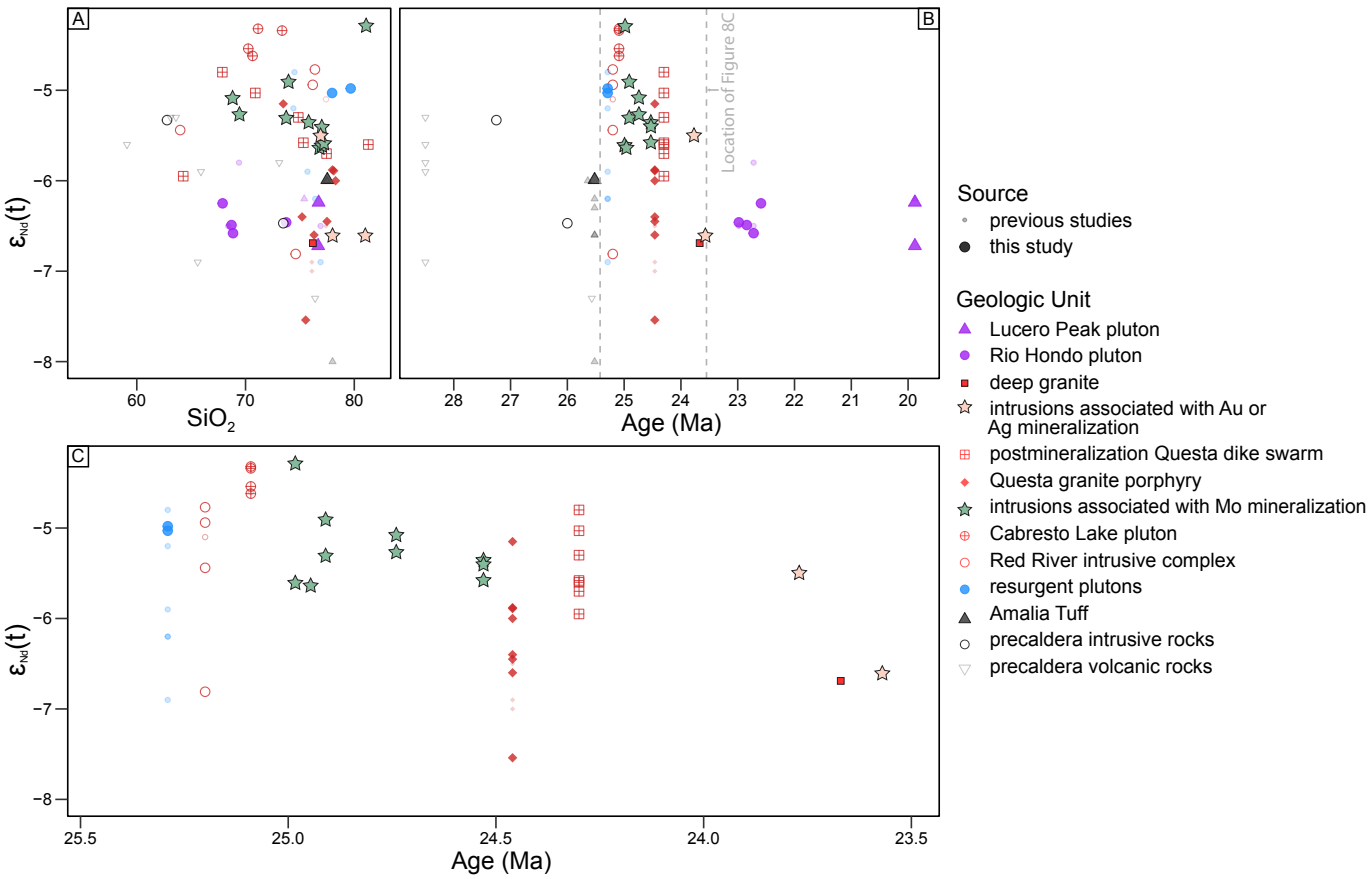

Fig. 8. $\varepsilon_{Nd}(t)$ compositions of igneous rocks from the Latir magmatic center throughout its evolution, relative to SiO_2 composition (wt %; A) and relative to time (B and C). There is not a clear relationship between SiO_2 content and Nd isotope composition, but there are distinct differences in the composition of different magmatic pulses through time. Dashed lines in (B) indicate the region shown in (C). Includes data from Johnson et al. (1990). Previous data from Thompson et al. (1986) and Johnson et al. (1990). Ages from Table 1. Note that all previously published data are shown in a smaller symbol class than the new data presented here.

during assembly of the Questa Mo deposit and reaches least radiogenic compositions during intrusion of the Questa granite porphyry (Figs. 8, 10). The approximately 24.5 Ma post-Mo–mineralization dike suite in the Questa Mo deposit area has $\varepsilon_{Nd}(t)$ values closer to the older mineralizing intrusions, but these values are distinct from the 23.8 Ma deep granite that intruded below the Questa Mo deposit (Fig. 3), which has less radiogenic Nd compositions than the unmineralized dike suite in the vicinity of the Questa Mo deposit (Fig. 8). The 23.7 Ma dikes from the hydrothermally altered Junebug scar and Silver Tip Group of mines associated with Ag and/or Au mineralization along the southern caldera margin have Nd isotope compositions that are indistinguishable from the deep granite sampled below the Questa deposit. The Rio Hondo and Lucero Peak plutons and the associated silicic dikes that intruded south of the caldera margin after approximately 23.7 Ma have more restricted ranges of isotope ratios ($^{87}Sr/^{86}Sr_i$ = 0.7046 to 0.7060; $\varepsilon_{Nd}(t)$ = –6.24 to –6.72; $^{206}Pb/^{204}Pb_i$ = 17.35 to 17.56; Figs. 7–9).

Previous studies of the Latir magmatic center interpreted some of the isotopic variability to be related to up to 50% assimilation of upper crustal rocks (Johnson et al., 1990). However, we consider it unlikely that variations in isotopic geochemistry through time are the result of significant upper crustal assimilation because the geochronologic data are inconsistent with individual plutons extracted from a single, large, evolving magma chamber (e.g., Tappa et al., 2011; Gaynor et al., 2019b). Moreover, thermodynamic calculations indicate that a high degree of assimilation is energetically inefficient and induces crystallization of the magma (Glazner, 2007). Piecemeal assembly of the batholith by smaller intrusive pulses and thermal limitations of volumetrically significant upper crustal assimilation suggest the effects of assimilation are minor (e.g., Glazner and Bartley, 2006), and mostly likely localized in individual pulses.

We suggest that the Questa batholith within the Latir magmatic center was episodically assembled after ignimbrite eruption, and that much of the isotopic variation is the result of fluctuations in a deep crustal hot zone (e.g., Annen et al., 2006). These fluctuations include a mixture of ancient deep crust, juvenile mafic crust, and mantle-derived melts and fluids based on the heterogeneous isotope geochemistry (Figs. 6–10). Previous work in the Latir magmatic center suggests that mantle-derived mafic melts played an important role in delivering heat and transferring material into the lower crust, but different igneous units incorporated different degrees of crustal materials (Johnson et al., 1990). Melts generated in this deep crustal zone interact with preexisting lower crust

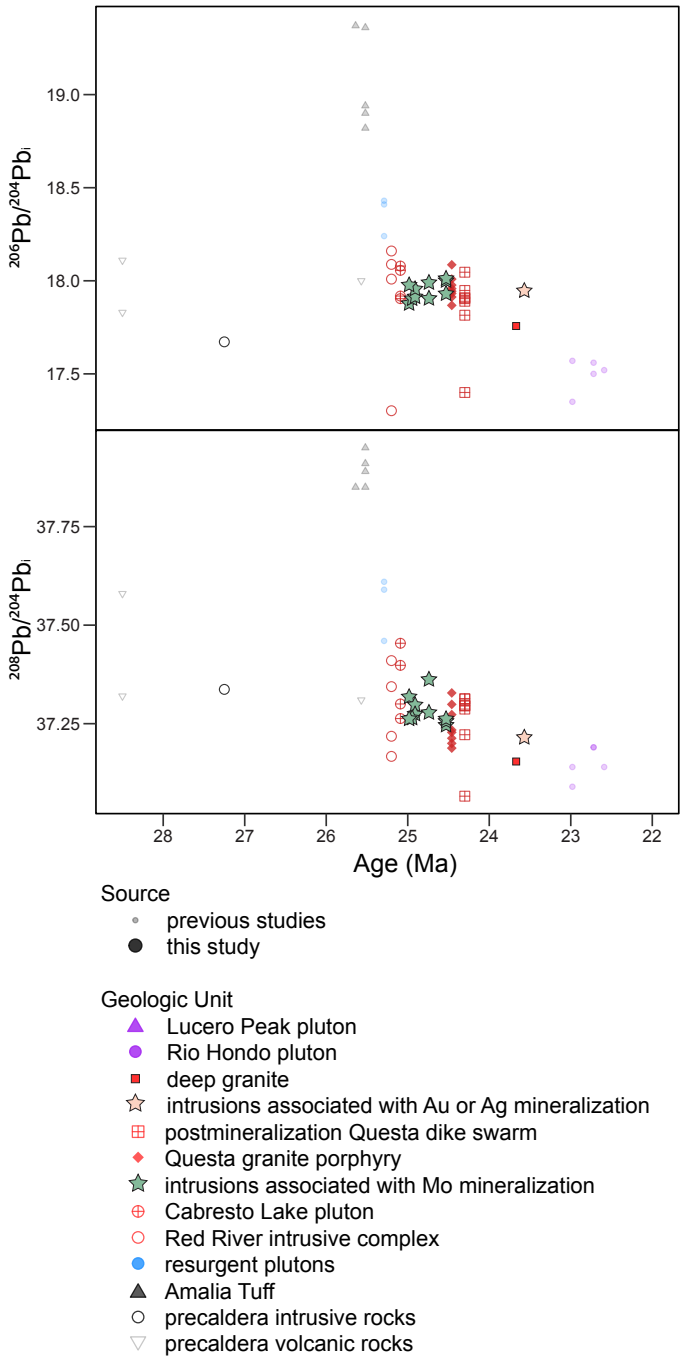

Fig. 9. Initial Pb isotope compositions of magmatic rocks from the Latir magmatic center. Includes data from Johnson and Lipman (1988) and Johnson et al. (1989, 1990). Ages from Table 1. Note that all previously published data are shown in a smaller symbol class than the new data presented here.

to generate hybrid magmas that subsequently ascend into the shallower crust. In this model, major and trace element variations reflect a combination of inheritance from source material and subsequent crystal-liquid separation processes in the upper crust (e.g., Bons et al., 2004; Coleman et al., 2012; Clemens and Stevens, 2012), whereas variations in radiogenic isotopes are dominantly controlled by deep crustal interaction between juvenile mafic melts and preexisting crust (e.g., Annen et al., 2006). This variable influence of juvenile material is best represented by the variable $\varepsilon_{Nd}(t)$ compositions throughout the evolution of the magmatic center, ranging almost four epsilon units over 10 m.y., including a rapid shift over hundreds of k.y. following the eruption of the Amalia Tuff (Fig. 8).

Climax-type mineralization in the context of a long-lived silicic magma center

Within the Latir magmatic center, early plutons were assembled under conditions favorable for porphyry Mo mineralization. These conditions include (1) intruding into a shallow environment (<6 km; Cline and Bodnar, 1994; Gaynor et al., 2019b); (2) intruding immediately after the transient high magma flux episode that formed the Questa caldera (Tappa et al., 2011; Gaynor et al., 2019b); and (3) a high volatile flux as suggested by the occurrence of peralkaline phases potentially evolved from crystallization of mafic magmas deeper in the system (Johnson et al., 1989). Favorable conditions for Mo mineralization are supported by the high concentrations of silica and incompatible elements such as Nb, Y, and Rb, and depletion of Sr—all characteristic of Climax-type mineralization (Carten et al., 1993; Ludington and Plumlee, 2009). In fact, the earliest plutons to intrude the caldera contain the highest Nb and Y and lowest Sr concentrations observed in the batholith. Despite these favorable conditions and chemical signatures characteristic of mineralization, the early plutons lack any appreciable mineralization or even wall-rock alteration, and it is unlikely that any mineralization or alteration has been lost to erosion (Audétat and Pettke, 2003).

The mineralizing intrusions at the Questa deposit have lower abundances of Nb and Y and lower Rb/Sr than the plutons that intruded immediately before and after mineralization (caldera margin plutons, Questa granite porphyry; Figs. 5, 6). These data highlight that, even within the context of coeval silicic magmas, mineralizing intrusions in porphyry Mo deposits might not have the greatest enrichments in HFSEs in their broader magmatic system. Furthermore, these intrusions do not all have the major element compositions of high-silica rhyolites (Fig. 4). In particular, the dark matrix porphyry is more intermediate in composition (SiO_2 = 69%) and is closely associated with high-grade mineralization and alteration throughout the deposit (Figs. 1, 4; Ross et al., 2002; Gaynor et al., 2019a). That is, silicic magmas were injected into shallow porphyry environments over millions of years in the Latir magmatic center, but mineralization was punctuated and not necessarily associated with the largest degrees of differentiation. This observation could have significant implications for how porphyry Mo deposits are targeted geochemically within long-lived silicic magma centers, as Nb and Y enrichments may not necessarily associate with Mo mineralization.

Evaluation of existing models describing porphyry Mo mineralization

The evidence for brief pulses of porphyry-related mineralization during the prolonged assembly of the Questa batholith, in conjunction with evidence for temporal shifts in the composition of magma sources, have important implications for genetic models of the Questa Mo deposit. Models that have been proposed to explain the origin of Mo mineralization at Questa and in similar Climax-type deposits include (1) deriva-

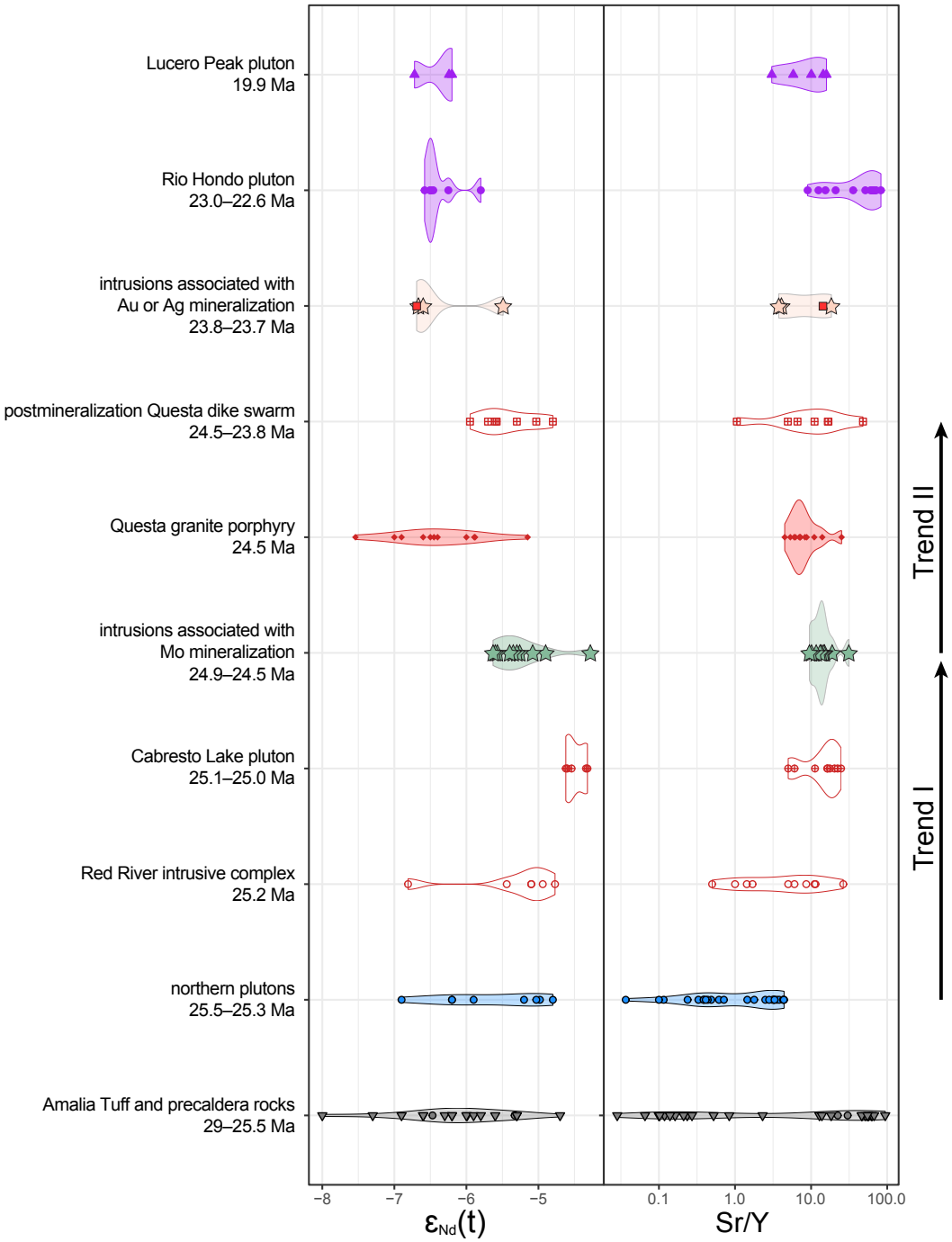

Fig. 10. Violin plot of $\varepsilon_{Nd}(t)$ and Sr/Y geochemistry of igneous rocks from the Latir magmatic center, highlighting the temporal variability throughout the evolution of the center. Magmatic periods associated with mineralization are geochemically distinct from earlier and later intrusions, indicating that mineralization within the Latir magmatic center is driven by changes in magma genesis. See text for discussion. Published data from Johnson and Lipman (1988) and Johnson et al. (1989, 1990). Ages from Table 1.

tion of mineralizing intrusions from juvenile mantle-derived sources (e.g., Rosera et al., 2013); (2) melting of ancient felsic crustal rocks (e.g., Farmer and DePaolo, 1984; Stein, 1985; Stein and Crock, 1990); and (3) upper crustal differentiation of magmas with chemical characteristics similar to the Cabresto Lake pluton (e.g., Johnson et al., 1990; Klemm et al., 2008; Greber et al., 2014). Alternatively, we suggest that (4) fluctuations in a deep crustal hot zone were responsible for the timing and presence of Mo mineralization at Questa.

Juvenile mantle-derived origin: Recent work hypothesized that Mo mineralization at Questa was optimized because it followed a caldera-forming ignimbrite sequence. Rosera et al. (2013) proposed a model wherein ignimbrite formation was associated with intrusion of mantle-derived melts into the

lower crust, creating a zone of hybridized lower crust composed of juvenile mafic rocks, hydrothermal assemblages, and preexisting lower crust. This work hypothesized that postignimbrite, lower crustal anatexis occurred in a region that had been recharged with mantle-derived volatiles, giving it the ability to produce volatile-rich, mineralizing magmas (Rosera et al., 2013). This model incorporates the following observations about Climax-type Mo deposits and their associated magmas: (1) these deposits commonly form in close spatio-temporal proximity to ignimbrite vents (e.g., Keith et al., 1986; Hulen et al., 1987; Rosera et al., 2013, 2021; Mercer et al., 2015b); (2) Pb and S isotope data indicate that a mantle component was present in the magma genesis and metallogenesis of many of these porphyry Mo systems (e.g., Stein, 1985; Stein and Hannah, 1985; Pettke et al., 2010); (3) geochemical and experimental studies have shown that partial melting of hydrous lower crust can generate appreciable volumes of felsic magmas, similar to mineralizing magmas at Questa, capable of ascension to the upper crust (e.g., Mahood and Halliday, 1988; Ratajeski et al., 2005; Sisson et al., 2005).

One testable prediction of this model is that mineralizing intrusions should have isotopic compositions most comparable to juvenile mantle-derived material. Neodymium isotopes serve as the best test for this, as they are less sensitive to the effects of alteration (e.g., Farmer and DePaolo, 1984) and record magma genesis from before, during, and after mineralization. A juvenile mantle-derived origin hypothesis does not match the whole-rock isotope geochemistry from the Latir magmatic center; as the most juvenile Nd isotopes in the postcaldera sequence are from the immediately pre-Mo, barren Cabresto Lake pluton and a single sample of the central aplite (the first pulse of mineralizing magmas at Questa). The central aplite from the Questa porphyry Mo deposit is associated with a relatively low-grade ore zone (<0.1 wt % MoS_2; Gaynor et al., 2019a). The bulk of the high-grade Mo orebodies (>0.2 wt % MoS_2) formed during intrusion of subsequent magmas, and those intrusions have less radiogenic $\varepsilon_{Nd}(t)$ compositions, indicating that the most juvenile magmas were not responsible for mineralization (Figs. 8, 10). Therefore, whereas Mo-mineralization in these systems may involve more juvenile input than other magmas from temporally related batholiths, a sudden, higher flux of juvenile input is unlikely to serve as the mechanism for deposit formation. This interpretation also rules out differentiation of melts derived from metasomatized continental lithospheric mantle (Pettke et al., 2010), again because the most juvenile magmas predate mineralization at Questa.

Ancient felsic lower crust: Early radiogenic isotope studies of Climax-type deposits in Colorado suggested that the mineralizing intrusions are sourced from ancient intermediate to felsic lower crust (Farmer and DePaolo, 1984; Stein, 1985; Stein and Crock, 1990). These deposits have relatively nonradiogenic Nd compositions (ε_{Nd} = -9 to -14) and variable Pb isotopic compositions consistent with high Th/U sources ($^{206}Pb/^{204}Pb_i$ = 17.3–17.6; $^{208}Pb/^{204}Pb_i$ = 38–39.5; Stein, 1985; Stein and Crock, 1990). However, the data for mineralizing intrusions from Questa do not overlap the values for Climax-type deposits from Colorado. The $\varepsilon_{Nd}(t)$ values are higher (–4.28 to –5.66), and the Pb isotope data ($^{206}Pb/^{204}Pb_i$ = 17.78–18.01; $^{208}Pb/^{204}Pb_i$ = 37.25–37.36) are indicative of source rocks with much lower Th/U compositions than the other Climax-type deposits. Furthermore, the original interpretation that Climax-type intrusions require anatexis of ancient felsic crust has been challenged by recent chemical and isotopic studies of deep crustal xenoliths and Eocene-Oligocene granites and rhyolites. These newer studies suggest that lower crust in Colorado is mafic in composition and enriched in F, and they suggest that F-rich Mo mineralization is related to melting of ancient mafic, rather than felsic, crust (Farmer et al., 2005; Jacob et al., 2015; Rosera et al., in press). Seismic refraction data in the southern Rocky Mountains also demonstrate that the lower crust in the region (below ~25 km) is also more consistent with dense mafic rocks rather than felsic material (Snelson et al., 2005). Consequently, any deep source for primitive magmas for the porphyry system would have more likely melted ancient rocks with more basaltic compositions. Magma generation from felsic source rocks is therefore unlikely a dominant mechanism in the formation of Questa porphyry Mo deposit.

Crystal fractionation of magmas similar to the Cabresto Lake pluton: Previous work on the Latir magma center interpreted that porphyry Mo and polymetallic vein mineralization along the southern caldera rim was associated with magmas emanating from a large, actively fractionating magma body in the upper crust (e.g., Johnson et al., 1990; Klemm et al., 2008; Greber et al., 2014). These models are largely based on chemical trends (isotopic or elemental) that were assumed to fit a time-progressive model (e.g., crystal fractionation drives incompatible elements towards higher abundances through time). However, these observations are difficult to reconcile with new observations of the complex intrusive history of the Questa porphyry Mo deposit (Rosera et al., 2013; Gaynor et al., 2019a). For example, Johnson et al. (1989) suggested that the Mo-mineralizing intrusions at the Questa porphyry deposit were derived by crystal fractionation of parental magmas similar to the monzongranite from the Cabresto Lake pluton (71 wt % SiO_2). However, their model used the Bear Canyon and Sulphur Gulch plutons as compositions representative of the Questa Mo deposit, whereas new geochronology and detailed structural mapping of intrusions indicate that those plutons intruded after the bulk of high-grade porphyry Mo mineralization at Questa (Gaynor et al., 2019a).

Our geochemical data also preclude derivation of the mineralizing intrusions from primitive magmas comparable to the most mafic intrusions in the Cabresto Lake pluton (e.g., Johnson et al., 1989). The mineralizing intrusions have lower Nb and Y and higher Th than samples with comparable silica content from the Cabresto Lake pluton (Figs. 5, 6). Distinct Nd isotope compositions between the Cabresto Lake pluton and mineralizing intrusions rules out any interpretation that different trace element patterns are simply the result of crystallizing assemblages that prefer Nb and Y. A simpler explanation is that the mineralizing intrusions are from a slightly younger and compositionally distinct batch of magmas that had little to no interaction with the magmas that formed the Cabresto Lake pluton.

Deep crustal hot zone with variable magma flux: None of the models presented above are entirely satisfactory for explaining the origin of mineralizing intrusions in the Questa porphyry Mo deposit. There is no strong evidence identifying a single

source for the magmas that contributed to the Questa porphyry Mo deposit. Instead, mineralization appears to have occurred during a change in source contributions, in particular as the system moved away from its most juvenile "peak" (in terms of $\varepsilon_{Nd}(t)$), which we describe as the inflection between Trend I and Trend II on Figure 10. These data, in conjunction with the observations discussed above, suggest that mineralization depends on dynamics between juvenile, mantle-derived melts, and deep ancient crustal sources (Fig. 11).

In the Latir magmatic center, magma flux varied from high (ignimbrite stage) to low (batholith assembly; Tappa et al., 2011; Gaynor et al., 2019b), with mineralization occurring episodically during batholith assembly. Numerical models suggest that magma flux into the upper crust can help drive porphyry-related mineralization (Chelle-Michou et al., 2017; Korges et al., 2020), and the magmas that reach the upper crust are generated in a deep crustal hot zone (e.g., Chiaradia and Caricchi, 2017). We propose that, in the case of the Questa porphyry Mo deposit, generation of primary silicic magmas from the deep crust was, in part, controlled by fertility of wall rocks that interacted with heat and fluids derived from the mantle. Intrusion of juvenile mafic magmas into the deep crust, such as those that drove the caldera-forming eruption (Johnson et al., 1990), modified portions of the lower crust by forming hybrid domains with crustal- and mantle-derived components. End-member compositions within these hybridized domains include juvenile mafic rocks, preexisting mafic lower crust (e.g., Snelson et al., 2005), and zones metasomatized by the large influx of mantle-derived melts and volatiles, including sulfur. Although mineralizing intrusions may not have been derived solely from juvenile mafic rocks, metasomatism of ancient lower-crust wall rocks can modify later partial melting events (e.g., metasomatized rocks will partially melt at lower temperatures). The composition and volume of anatectic melts from these hybridized lower crustal domains may vary through time. The resulting combinations of magma genesis, magma flux and volatile contents may trigger transient periods of mineralization between otherwise barren magmatism, which better explains the isotopic record of the Latir magmatic center.

These observations of short-lived, discrete mineralization events between periods of barren magmatism have also been noted in other porphyry systems. The majority of the ore of the Chalukou porphyry Mo deposit mineralized over a period of <650 k.y., between periods of barren magmatism (e.g., Zhao et al., 2021). Metal deposition at the Batu Hijau porphyry Cu-Au deposit occurred in less than 90 ± 32 k.y., followed by barren magmatism (Large et al., 2020). Copper mineralization at the Koloula porphyry prospect occurred over 50 k.y., only 150 k.y. after a period of barren magmatism (Tapster et al., 2016). Porphyry Cu formation at the Bajo de la Alumberera deposit occurred briefly over 19 ± 12 k.y., with barren magmatism immediately before and afterward, including significant explosive volcanism (Buret et al., 2016, 2017). Therefore, the discrete periods of mineralization observed at Questa may not be anomalous within mineralized volcano-plutonic complexes, and the record of changes in magma sourcing described here may also be expressed in other locations. The radiogenic isotope data from the Latir magmatic center indicate that these rapid fluctuations between barren and mineralized intrusions are (1) related to secular changes in magma source(s), and (2) no single end-member source may be tied directly to barren or mineralizing intrusions.

Magmas associated with porphyry and polymetallic vein mineralization

Although the Questa porphyry Mo deposit is historically the most important mineral deposit in the area, it is not the only magmatic-hydrothermal mineral system that developed during assembly of the volcano-plutonic complex (Figs. 1–3), and the long-term changes in magma sources in the region could also have implications for understanding the origins of these mineral prospects. A suite of silicic dikes intruded along the southern caldera margin after the collapse of the Questa caldera and are associated with polymetallic veins historically mined for Au, Ag, Pb, Zn, and Cu, but are all currently subeconomic (Fig. 1; McLemore and Mullen, 2004). High-precision zircon geochronology of these dikes indicates that the dike intrusion and associated mineralization occurred over multiple generations of discrete events (Gaynor et al., 2019b), and data presented in this study lends new insight into how these deposits relate to the broader magma system.

Greber et al. (2014) suggested the silicic dikes that intruded the southern caldera margin are late-stage melts tapped from a residual magma following assembly of the Questa Mo deposit. However, high-precision zircon geochronology indicates these dikes are approximately 800 k.y. younger than the last major pulse of Mo mineralization within the Questa deposit, and their zircon ages overlap with a subsurface, post-mineralization equigranular granite, deep beneath the Mo orebodies (Gaynor et al., 2019b; Fig. 3). Both the rhyolite dike associated with polymetallic mineralization near the Silver Tip group of mines and the rhyolite dike associated with high-temperature alteration in the Junebug core have Nd isotope compositions similar to the deep equigranular granite beneath the Questa porphyry Mo deposit ($\varepsilon_{Nd}(t) = -6.7$; Figs. 8, 10). Furthermore, gravity modeling indicates that the deep equigranular granite underlies the southern caldera margin, below the composite dike swarm that follows the caldera ring structure (Gaynor et al., 2019b). These data suggest that the equigranular granite and silicic dikes associated with polymetallic Au-Ag-Cu (Pb-Zn) mineralization along the southern margin are part of the same magma system (i.e., a pluton with dikes emanating from its top). However, this intrusion is distinct from those that built the slightly older Questa porphyry Mo deposit, and their Nd isotope compositions do not reflect the same source or mixture of source rocks.

Numerous low-grade polymetallic vein deposits also crop out a few kilometers south of the Questa caldera margin, within the region of the southern plutons and highlighted by the South Fork Au-Ag-Cu prospects (Fig. 1). The largest intrusion south of the caldera margin is the composite Rio Hondo pluton (22.98–22.59 Ma; Tappa et al., 2011). However, zircon U-Pb geochronology from the intrusions spatially associated with mineralization preclude the Rio Hondo pluton as the source for polymetallic mineralization south of the caldera margin, as the dikes associated with mineralization significantly predate the construction of the Rio Hondo pluton (Table 1; Fig. 2; Gaynor et al., 2019b). Rhyolite dikes associated with polymetallic veins south of the caldera yield slightly

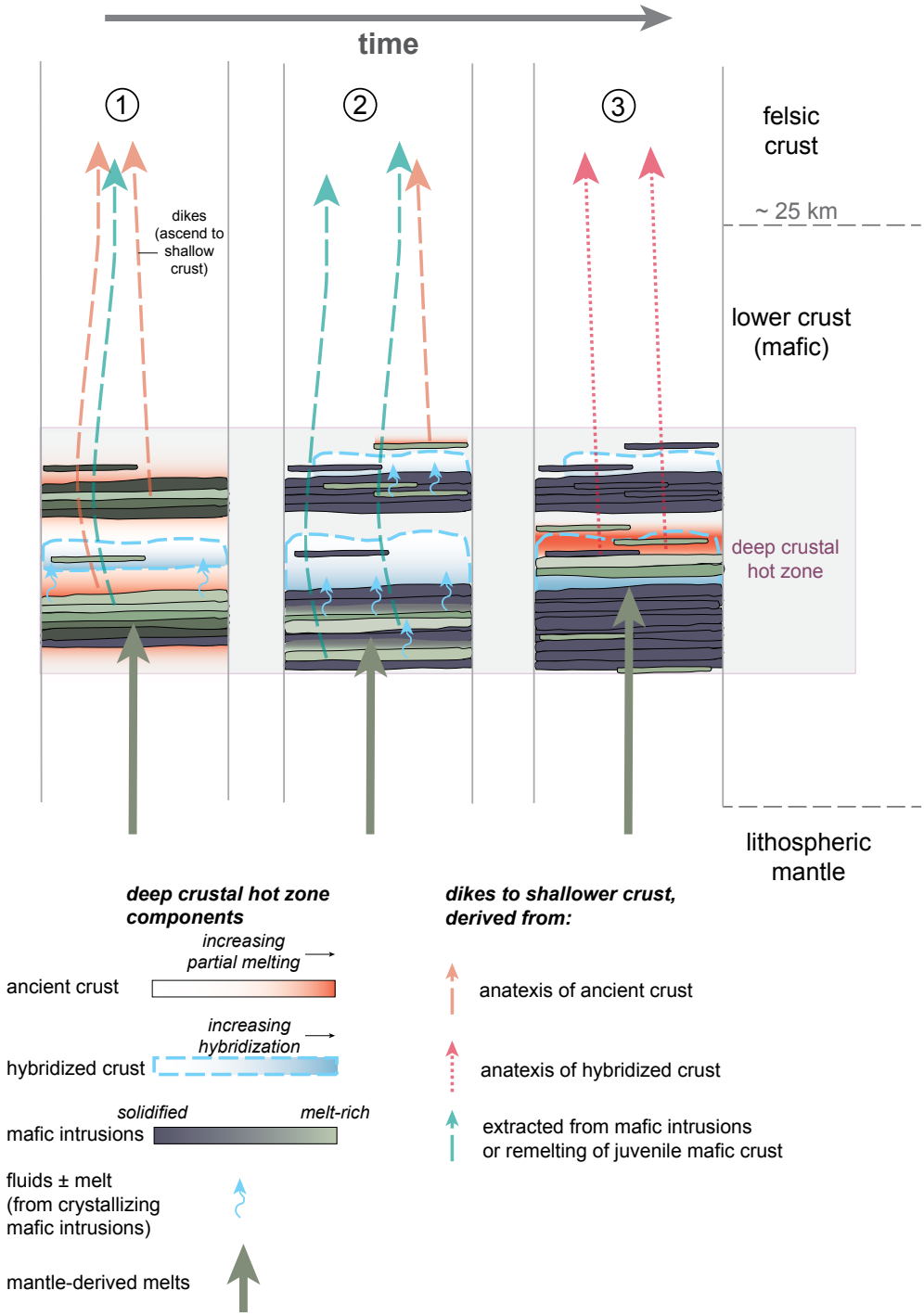

Fig. 11. Schematic cartoon showing how fluctuations in a deep crustal hot zone can create juvenile crust and melt and/or hybridize preexisting crust. Panel 1: Formation of a deep crustal hot zone by mafic, mantle-derived intrusions. Melts that ascend to shallower crust are extracted from either juvenile mafic magma systems (green) or generated by anatexis of ancient mafic lower crust (orange). Late-stage fluids and melt generated from deep mafic intrusions ascend into ancient crust and form a hybridized zone. Panel 2: Focusing of mantle-derived melts into juvenile mafic intrusions results in remelting of juvenile crust. Melts that ascend to the shallower crust from this stage have more juvenile isotopic compositions (i.e., higher $\varepsilon_{Nd}(t)$) than melts that incorporate ancient felsic crustal material. Solidification of mafic magmas in the deep crustal hot zone results in further hybridization of ancient crust, and possibly reenrichment of previously melted crust. Panel 3: A shift in the loci of mafic magmatism to a recently hybridized zone of ancient felsic crust. Partial melts generated from hybridized crust could melt at a different temperature, have different volatile load (i.e., melting metasomatized rocks), and melt at a different rate (i.e., outward flux) than melts generated from unmodified preexisting crust. Fluctuations between end-member melt sources in a deep crustal hot zone can therefore influence physical and chemical melt properties during shallow crustal batholith assembly and mineralization. Modified after Annen et al. (2006); depth of felsic-mafic crust transition from Snelson et al. (2005).

older zircon ages relative to the deep granite beneath the Questa deposit and have a more radiogenic Nd composition than the deep granite ($\varepsilon_{Nd}(t)$ = –5.5 and –6.7, respectively; Fig. 8), and thus, we consider it unlikely that these two units are derived from the same magma body. Instead, these data suggest that there was variability in isotopic compositions and ages of intrusion of various rhyolite dikes within and south of the caldera margin.

Broader implications for models of porphyry deposit formation

Commonly, porphyry deposits may be genetically associated with multiple metal associations, including polymetallic veins, stockworks, and replacement deposits (e.g., Hofstra and Kreiner, 2020). The structural expression of specific metal ore shells has been interpreted as a function of difference in style of exsolution (brine versus vapor) or solubility within a hydrothermal fluid (e.g., Hedenquist and Lowenstern, 1994; Sillitoe, 2010). Although this may be the case in systems where porphyry mineralization is driven by a single, or a few, large pulse(s) of magma, recent work found that Au endowments in Cu-Au porphyry deposits can be driven by chemical differences within magmas that influence the ability to extract metals from melt (Chiaradia, 2020). This observation highlights how geochemical variations during protracted porphyry assembly can change the metal expression. Importantly, our data suggest that these geochemical variations exist in magmas prior to ascent into the upper crust, and assembly of causative magma bodies related to porphyry deposits. This evidence suggests that metal endowment is potentially correlated to secular changes in sources and contributions of magmas. Temporally discrete changes in polymetallic associations have been observed in many porphyry belts with polymetallic associations, where long-lived, pulsed magmatism reflects distinct changes in tectonic and magmatic conditions that drive magmatic-hydrothermal mineralization (e.g., Zimmerman et al., 2008; Moritz et al., 2016; Rosera et al., 2021).

Several local-scale porphyry ore systems provide examples in which different metal associations or metal depositional events are associated with different batches of magma. The Bingham Canyon Cu-Au-Mo deposit is a particularly good example; polymetallic veins have been identified as postdating all explored plutonic bodies and porphyry Cu-Au mineralization, related either to the causative pluton for Mo mineralization or to a separate, unexplored intrusion (Tomlinson et al., 2021). Furthermore, the main period of Mo mineralization at the Bingham deposit occurred after emplacement of the last causative porphyry for Cu-Au ore (Large et al., 2021). In this case, the commonly observed "telescoping" of ore shells may not be purely a function of fluid evolution (e.g., Sillitoe, 2010), but rather rapid intrusion of geochemically different magmas. Furthermore, recent work on the Dawson Range Au belt in Canada has shown that least two separate porphyry systems, separated by 6 to 9 m.y., were responsible for the superposition and enrichment of the highest-grade porphyry deposits in the region (Lee et al., 2021).

Our data support the growing body of literature that indicates spatially coincident porphyry and polymetallic mineral deposits do not necessarily represent prograde fluid evolution from one or a few large upper crustal magma systems. In the Questa batholith, causative intrusions for polymetallic mineralization along the southern caldera margin are younger and isotopically distinct from the systems that built the Questa porphyry Mo deposit. In fact, the deep equigranular granite that underlies the Questa porphyry Mo deposit is equivalent in age and $\varepsilon_{Nd}(t)$ to rhyolite dikes associated with alteration and polymetallic mineralization along the southern caldera margin, but the pluton is unmineralized. Hence, there is no indication that a continuous system of Mo- to Ag-bearing mineralizing fluids existed at one time. These observations highlight the internal complexities that follow from incremental pluton assembly within less than 100-k.y. timescales, and they emphasize the need for careful mapping supplemented with high-precision geochronology to better match mineral patterns to causative magmas.

In regions hosting many different metals associated with different fugacity and volatile concentrations in ore, incremental emplacement of magmas from distinct sources may control discrete metal endowments, regardless of how they are structurally overprinted in a specific region. The traditional porphyry model is centered on a deep magma system in which the solubility of individual metal species dictates the structure of ore shells upon hydrothermal-magmatic exsolution (e.g., Sillitoe, 2010). This model can feasibly establish entire mineral systems and explain the development of structurally separated ore shells of different metals in a single porphyry system. However, a single, consolidated magma system is not required to form various polymetallic deposits around a given porphyry. Variations in magma compositions during the lifespan of upper crustal magma systems can yield differing styles of mineralization, creating different metal expressions which can either overprint or emplace separately within the upper crust, leaving behind a mineralization record without clear vectors to causative magmas. One mineral system does not necessarily equate to one magma system, and an understanding of porphyry mineralization on a deposit or regional scale requires detailed mapping and analyses to determine its genesis. As a result, we argue for a far more compartmentalized system, wherein distinct magmatic inputs tied to different compositions, volatile loads, metals, and rates of generation, are complexly tied to the expression of economic metal anomalies in the upper crust.

Conclusions

Geochemical data from the Latir magmatic center indicate that deep magma sources fluctuated through time, with individual metal expressions associated with geochemically and temporally distinct batches of magma. The geochemistry of the Questa Mo deposit is inconsistent with genetic models for the system in which large-scale fractionation of a single long-lived magmatic system is responsible for fluid evolution and mineralization, or models that rely on a significant juvenile mantle-derived input. Polymetallic mineralization along the southern caldera margin and a few kilometers to the south is related to silicic dikes that lack affinity to the intrusions associated with major Mo mineralization. The temporal changes in isotopic trends within the Latir magmatic center correspond to fundamental changes in the magmatic system following eruption of the 500-km^3 Amalia Tuff, and we hypothesize that these changes reflect substantial modification

and increasing complexity of the source of magmas in the lower crust. The distinct expression of porphyry magmatism within the Latir magmatic center reflects varying contributions from preexisting lower crust, juvenile lower crust, and metasomatic overprinting induced by an influx of volatiles and melt from the mantle. We suggest that future models of porphyry and associated polymetallic mineralization within long-lived magma centers incorporate the potential for these shifting conditions of magma genesis. That is, the full suite of mineral commodities in a porphyry mineral system are not necessarily the products of a simple, monogenetic magma system with metal zonation linked to prograde evolution of fluids from a single magma source; instead, they could represent superposed mineralization episodes from different magma sources through time. High-precision geochronology, robust geochemical data, and detailed field relations are all required to further test this hypothesis in other systems.

Acknowledgments

This project would not have been possible without the foundational work, mentorship, and help provided by the late Bruce Walker. Funding was provided by NSF EAR 1220252, awarded to Coleman, and the Geological Society of America, Sigma Xi Grants-in-Aid of Research, and the University of North Carolina Martin Fund awarded to Gaynor. Chevron Mining Inc. provided access to the Questa mine property, breakfast burritos, and drill core. Thanks to Allen Glazner for his support in XRF geochemistry. The ideas in this manuscript benefited from discussions with Connor Lawrence, Ryan Mills, Ryan Frazer, Steve Ludington, and Massimo Chiaradia. Thanks to Graham Lederer, Kathryn Watts, and Ben Williamson for constructive and very thorough reviews of this manuscript. Thanks to Editor Larry Meinert and Associate Editor Andreas Audetat for the handling of the manuscript. Any use of trade, firm, or product names is for descriptive purposes only and does not imply endorsement by the U.S. Government.

REFERENCES

Annen, C., Blundy, J.D., and Sparks, R.S.J., 2006, The genesis of intermediate and silicic magmas in deep crustal hot zones: Journal of Petrology, v. 47, p. 505–539.

Audétat, A., and Pettke, T., 2003, The magmatic-hydrothermal evolution of two barren granites: A melt and fluid inclusion study of the Rito del Medio and Canada Pinabete Plutons in northern New Mexico (USA): Geochimica et Cosmochimica Acta, v. 67, p. 97–121.

Bachmann, O., and Bergantz, G.W., 2004, On the origin of crystal-poor rhyolites: Extracted from batholithic crystal mushes: Journal of Petrology, v. 45, p. 1565–1582.

Bons, P.D., Arnold, J., Elburg, M.A., Kalda, J., Soesoo, A., and van Milligen, B.P., 2004, Melt extraction and accumulation from partially molten rocks: Lithos, v. 78, p. 25–42.

Buret, Y., von Quadt, A., Heinrich, C.A., Selby, D., Wälle, M., and Peytcheva, I., 2016, From a long-lived upper-crustal magma chamber to rapid porphyry copper emplacement: Reading the geochemistry of zircon crystals at Bajo de la Alumbrera (NW Argentina): Earth and Planetary Science Letters, v. 450, p. 120–131.

Buret, Y., Wotzlaw, J.F., Roozen, S., Guillong, M., von Quadt, A., and Heinrich, C.A., 2017, Zircon petrochronological evidence for a plutonic-volcanic connection in porphyry copper deposits: Geology, v. 45, p. 623–626.

Cameron, A.E., Smith, D.H., and Walker, R.L., 1969, Mass spectrometry of nanogram-size samples of lead: Anales Chemical, v. 41, p. 525–526.

Caricchi, L., Simpson, G., and Schaltegger, U., 2014, Zircons reveal magma fluxes in the Earth's crust: Nature, v. 511, p. 457–461.

Carten, R.B., Geraghty, E.P., Walker, B.M., and Shannon, J.R., 1988, Cyclic development of igneous features and their relationship to high-temperature hydrothermal features in the Henderson porphyry molybdenum deposit, Colorado: Economic Geology, v. 83, p. 266–296.

Carten, R.B., White, W.H., and Stein, H.J., 1993, High-grade granite-related molybdenum systems; classification and origin: Geological Association of Canada, Special Paper 30, p. 512–544.

Carter, L.C., Williamson, B.J., Tapster, S.R., Costa, C., Grime, G.W., and Rollinson, G.K., 2021, Crystal mush dykes as conduits for mineralising fluids in the Yerington porphyry copper district, Nevada: Communications Earth & Environment, v. 2, no. 1, p. 59.

Chelle-Michou, C., Rottier, B., Caricchi, L., and Simpson, G., 2017, Tempo of magma degassing and the genesis of porphyry copper deposits: Scientific Reports, v. 7, 12 p.

Chiaradia, M., 2015, Crustal thickness control on Sr/Y signatures of recent arc magmas: an Earth scale perspective: Scientific Reports, v. 5, article no. 8115.

——2020, Gold endowments of porphyry deposits controlled by precipitation efficiency: Nature Communications, v. 11, article no. 248.

Chiaradia, M., and Caricchi, L., 2017, Stochastic modelling of deep magmatic controls on porphyry copper deposit endowment: Scientific Reports, v. 7, article no. 44523.

Chiaradia, M., Merino, D., and Spikings, R., 2009, Rapid transition to long-lived deep crustal magmatic maturation and the formation of giant porphyry-related mineralization (Yancocha, Peru): Earth and Planetary Science Letters, v. 288, p. 505–515.

Chiaradia, M., Ulianov, A., Kouzmanov, K., and Beate, B., 2012, Why large porphyry Cu deposits like high Sr/Y magmas?: Scientific Reports, v. 2, article no. 685.

Chiaradia, M., Schaltegger, U., Spikings, R., Wotzlaw, J.F., and Ovtcharova, M., 2013, How accurately can we date the duration of magmatic-hydrothermal events in porphyry systems?: An invited paper: Economic Geology, v. 108, p. 565–584.

Clemens, J.D., and Stevens, G., 2012, What controls chemical variation in granitic magmas?: Lithos, v. 134–135, p. 317–329.

Cline, J.S., and Bodnar, R.J., 1994, Direct evolution of a brine from a crystallizing silicic melt at Questa, New Mexico, molybdenum deposit: Economic Geology, v. 89, p. 1780–1802.

Coleman, D.S., Gray, W., and Glazner, A.F., 2004, Rethinking the emplacement and evolution of zoned plutons: Geochronologic evidence for incremental assembly of the Tuolumne Intrusive Suite, California: Geology, v. 32, p. 433–436.

Coleman, D.S., Bartley, J.M., Glazner, A.F., and Pardue, M.J., 2012, Is chemical zonation in plutonic rocks driven by changes in source magma composition or shallow-crustal differentiation?: Geosphere, v. 8, p. 1568–1587.

Cox, D., Watt, S.F.L., Jenner, F.E., Hastie, A.R., Hammon, S.J., and Kunz, B.E., 2020, Elevated magma fluxes deliver high-Cu magmas to the upper crust: Geology, v. 48, p. 957–960.

Davis, D.W., Gray, J., Gumming, G.L., and Baadsgaard, H., 1977, Determination of the ^{87}Rb decay constant: Geochimica Cosmochimica Acta, v. 41, p. 1745–1749.

Farmer, G., and DePaolo, D., 1984, Origin of Mesozoic and Tertiary granite in the western United States and implications for pre-Mesozoic crustal structure 2. Nd and Sr isotopic studies of unmineralized and Cu- and Mo-mineralized granite in the Precambrian Craton: Journal of Geophysical Research, v. 89, p. 10,141–10,160.

Farmer, G., Broxton, D.E., Warren, R.G., and Pickthorn, W., 1991, Nd, Sr, and O isotopic variations in metaluminous ash-flow tuffs and related volcanic rocks at the Timber Mountain/Oasis Valley caldera complex, SW Nevada: Implications for the origin and evolution of large-volume silicic magma bodies: Contributions to Mineralogy and Petrology, v. 109, p. 53–68.

Farmer, G.L., Bowring, S.A., Williams, M.L., Christensen, N.I., Matzel, J.P., and Stevens, L., 2005, Contrasting lower crustal evolution across an Archean: Proterozoic suture: Physical, chemical and geochronologic studies of lower crustal xenoliths in southern Wyoming and northern Colorado: American Geophysical Union, Monograph 154, p. 139–162.

Gaynor, S.P., 2018, Modification of the crust: Mineralization and alteration in long-lived magmatic centers: Ph.D. thesis, Chapel Hill, University of North Carolina at Chapel Hill, 180 p.

Gaynor, S.P., Rosera, J.M., and Coleman, D.S., 2019a, Intrusive history of the Oligocene Questa porphyry molybdenum deposit, New Mexico: Geosphere, v. 15, p. 548–575.

Gaynor, S.P., Coleman, D.S., Rosera, J.M., and Tappa, M.J., 2019b, Geochronology of a Bouguer gravity low: Journal of Geophysical Research: Solid Earth, v. 124, p. 2457–2468.
Glazner, A.F., 2007, Thermal limitations on incorporation of wall rock into magma: Geology, v. 35, p. 319-322.
Glazner, A.F., and Bartley, J.M., 2006, Is stoping a volumetrically significant pluton emplacement process?: Geological Society of America Bulletin, v. 118, nos. 9–10, p. 1185–1195.
Gonzales, D.A., and Lake, E.T., 2016, Geochemical constraints on mantle-melt sources for Oligocene to Pleistocene mafic rocks in the Four Corners region, USA: Geosphere, v. 13, p. 201–226.
Greber, N.D., Pettke, T., and Nagler, T.F., 2014, Magmatic-hydrothermal isotope fractionation and its relevance to the igneous crustal signature: Lithos, v. 190–191, p. 104–110.
Hagstrum, J.T., and Johnson, C.M., 1986, A paleomagnetic and stable isotope study of the pluton at Rio Hondo near Questa, New Mexico: Implications for CRM related to hydrothermal alteration: Earth and Planetary Science Letters, v. 78, p. 296–314.
Harvey, J., and Baxter, E.F., 2009, An improved method for TIMS high precision neodymium isotope analysis of very small aliquots (1-10 ng): Chemical Geology, v. 258, p. 251–257.
Hedenquist, J.W., and Lowenstern, J.B., 1994, The role of magmas in the formation of hydrothermal ore deposits: Nature, v. 370, p. 519–527.
Heinrich, C.A., Driesner, T., Stefánsson, A., and Seward, T.M., 2004, Magmatic vapor contraction and the transport of gold from the porphyry environment to epithermal ore deposits: Geology, v. 32, p. 761–764.
Hofstra, A.H., and Kreiner, D.C., 2020, Systems-deposits-commodities-critical minerals table for the earth mapping resources initiative: U.S. Geological Survey, Open-File Report 2020-1042, http://pubs.er.usgs.gov/publication/ofr20201042.
Hulen, J.B., Nielson, D.L., Goff, F., Gardner, J.N., and Charles, R.W., 1987, Molybdenum mineralization in an active geothermal system, Valles caldera, New Mexico: Geology, v. 15, p. 748–752.
Ishikawa, Y., Sawaguich, T., Iwayi, S., and Horiuchi, M., 1976, Delineation of prospecting targets for Kuroko deposits based on modes of volcanism of underlying dacite and alteration halos: Mining Geology, v. 26, p. 105–117.
Jacob, K.H., Farmer, G.L., Buchwaldt, R., and Bowring, S.A., 2015, Deep crustal anatexis, magma mixing, and the generation of epizonal plutons in the Southern Rocky Mountains, Colorado: Contributions to Mineralogy and Petrology, v. 169, no. 7, article no. 7.
Jaffey, A.H., Flynn, K.F., Glendenin, L.E., Bentley, W.C., and Essling, A.M., 1971, Precision measurement of the half-lives and specific activities of ^{235}U and ^{238}U: Physical Review C, v. 4, p. 1889–1906.
Jochum, K.P., Weis, U., Schwager, B., Stoll, B., Wilson, S.A., Haug, G.H., Andreae, M.O., and Enzweiler, J., 2015, Reference values following ISO guidelines for frequently requested rock reference materials: Geostandards and Geoanalytical Research, v. 40, p. 333–350.
Johnson, C.M., 1991, Large-scale crust formation and lithosphere modification beneath Middle to Late Cenozoic calderas and volcanic fields, western North America: Journal of Geophysical Research, v. 96, p. 13485–13507.
Johnson, C.M., and Lipman, P.W., 1988, Origin of metaluminous and alkaline volcanic rocks of the Latir volcanic field, northern Rio Grande rift, New Mexico: Contributions to Mineralogy and Petrology, v. 100, p. 107–128.
Johnson, C.M., Czamanske, G.K., and Lipman, P.W., 1989, Geochemistry of intrusive rocks associated with the Latir volcanic field, New Mexico, and contrasts between evolution of plutonic and volcanic rocks: Contributions to Mineralogy and Petrology, v. 103, p. 90–109.
Johnson, C.M., Lipman, P.W., and Czamanske, G.K., 1990, H, O, Sr, Nd and Pb isotope geochemistry of the Latir volcanic field and cogenetic intrusion, New Mexico, and relations between evolution of a continental magmatic center and modifications of the lithosphere: Contributions to Mineralogy and Petrology, v. 104, p. 99–124.
Jones, D.M., 1990, Mid-Tertiary arcuate dikes and faults of the Rio Hondo-Red River drainages, Sangre de Cristo Mountains, New Mexico: A postulated outlying ring-fracture zone to the Miocene Questa caldera: New Mexico Geological Society, Field Conference Guidebook, v. 41, p. 365–368.
Keith, J.D., Shanks, W.C., III, Archibald, D.A., and Farrar, E., 1986, Volcanic and intrusive history of the Pine Grove porphyry molybdenum system, southwestern Utah: Economic Geology, v. 81, p. 553–577.
Klemm, L., Pettke, T., and Heinrich, C.A., 2008, Fluid and source magma evolution of the Questa porphyry Mo deposit, New Mexico, USA: Mineralium Deposita, v. 43, p. 533–552.
Korges, M., Wies, P., and Anderson, C., 2020, The role of incremental magma chamber growth on ore formation in porphyry copper systems: Earth and Planetary Science Letters, v. 552, 13 p.
Large, S.J.E., Wotzlaw, J.F., Guillong, M., von Quadt, A., and Heinrich, C.A., 2020, Resolving the timescales of magmatic and hydrothermal processes associated with porphyry deposit formation using zircon U-Pb petrochronology: Geochronology, v. 2, p. 209–230.
Large, S.J.E., Buret, Y., Wotzlaw, J.F., Karakas, O., Guillong, M., von Quadt, A., and Heinrich, C.A., 2021, Copper-mineralised porphyries sample the evolution of a large-volume silicic magma reservoir from rapid assembly to solidification: Earth and Planetary Science Letters, v. 563, 12 p.
Lee, C.T.A., and Tang, M., 2020, How to make porphyry copper deposits: Earth and Planetary Science Letters, v. 529, 11 p.
Lee, W.S., Kontak, D.J., Richards, J.P., Barresi, T., and Creaser, R.A., 2021, Superimposed porphyry systems in the Dawson Range, Yukon: Society of Economic Geologists, Special Publication 24, p. 29–48.
Li, X.C., Zhou, M.F., Yang, Y.H., Zhao, X.F., and Gao, J.F., 2018, Disturbance of the Sm-Nd isotopic system by metasomatic alteration: A case study of fluoroapatite from the Sin Quyen Cu-LREE-Au deposit, Vietnam: American Mineralogist, v. 103, p. 1487–1496.
Lipman, P.W., and Reed, J.C., 1989, Geologic map of the Latir volcanic field and adjacent areas, northern New Mexico: U.S. Geological Survey, Map I-1907, scale 1:48,000.
Lipman, P.W., Mehnert, H.H., and Naeser, C.M., 1986, Evolution of the Latir volcanic field, northern New Mexico, and its relation to the Rio Grande rift, as indicated by potassium-argon and fission track dating: Journal of Geophysical Research, v. 91, p. 6329–6345.
Livo, K.E., and Clark, R.N., 2002, Mapped minerals at Questa, New Mexico, using airborne visible-infrared imaging spectrometer (AVIRIS) data- Preliminary Report: U.S. Geological Survey, Open-File Report 02-0026, 13 p.
Ludington, S., and Plumlee, G.S., 2009, Climax-type porphyry molybdenum deposits: U.S. Geological Survey, Reston, 16 p.
Ludington, S., Briggs, J.P., and Robertson, J.M., 1983, Mineral resource potential of the Columbine-Hondo Wilderness Study Area, Taos County, New Mexico: US Geological Survey, USGS Numbered Series, no. 1570, Miscellaneous Field Studies Map MF-1570-A.
Lugmair, G.W., and Marti, K., 1978, Lunar initial $^{143}Nd/^{144}Nd$: Differential evolution of the lunar crust and mantle: Earth and Planetary Science Letters, v. 39, p. 349–357.
Lundblad, S.P., 1994, Evolution of carbonate platforms in the Umbria-Marche Apennines, Italy: Ph.D. dissertation, Chapel Hill, University of North Carolina at Chapel Hill, 145 p.
Mahood, G.A., and Halliday, A.N., 1988, Generation of high-silica rhyolite: A Nd, Sr, and O isotopic study of Sierra La Primavera, Mexican Neovolcanic Belt: Contributions to Mineralogy and Petrology, v. 100, p. 183–191.
Mathieu, L., 2018, Quantifying hydrothermal alteration: A review of methods: Geosciences, v. 8, no. 7, 27 p.
McLemore, V.T., and Mullen, K.E., 2004, Mineral resources in Taos County, New Mexico: New Mexico Geological Society, Guidebook, v. 55, p. 383–309.
McLemore, V.T., and North, R.M., 1984, Occurrences of precious metals and uranium along the Rio Grande rift in northern New Mexico: New Mexico Geological Society, Field Conference Guidebook, 35th Field Conference, p. 205–212, https://doi.org/10.56577/FFC-35.205.
Mercer, C.N., Reed, M.H., and Mercer, C.M., 2015a, Timescales of porphyry Cu deposit formation: Insights from titanium diffusion in quartz: Economic Geology, v. 110, p. 587–602.
Mercer, C.N., Hofstra, A., Todorov, T.I., Roberge, J., Burgisser, A., Adams, D.T., and Cosca, M., 2015b, Pre-eruptive conditions of the Hideaway Park topaz rhyolite: Insights in metal source and evolution of magma parental to the Henderson porphyry molybdenum deposit, Colorado: Journal of Petrology, v. 56, p. 645–679.
Meyer, J., and Foland, K.A., 1991, Magmatic-tectonic interaction during early Rio Grande Rift extension at Questa, New Mexico: Geological Society of America Bulletin, v. 103, p. 993–1006.
Michel, J., Baumgartner, L., Putlitz, B., Schaltegger, U., and Ovtcharova, M., 2008, Incremental growth of the Patagonian Torres del Paine laccolith over 90 k.y.: Geology, v. 36, p. 459–462.
Miller, R.B., and Paterson, S.R., 1999, In defense of magmatic diapirs: Journal of Structural Geology, v. 21, p. 1161–1173.
Moritz, R., Rezeau, H., Ovtcharova, M., Tayan, R., Melkonyan, R., Hovakimyan, S., Ramazanov, V., Selby, D., Ulianov, A., Chiaradia, M., and Putlitz, B., 2016, Long-lived, stationary magmatism and pulsed porphyry systems during Tethyan subduction to post-collision evolution in the southernmost

Lesser Caucasus, Armenia and Nakhitchevan: Gondwana Research, v. 37, p. 465–503.
Olsen, K.H., Baldridge, W.S., and Callender, J.F., 1987, Rio Grande rift: An overview: Tectonophysics, v. 143, p. 119–139.
Parrish, R.R., Roddick, J.C., Loveridge, W.D., and Sullivan, R.W., 1987, Uranium-lead analytical techniques at the geochronology laboratory: Geological Survey of Canada, Paper, v. 87, p. 3–7.
Pasteris, J.D., 1996, Mount Pinatubo volcano and "negative" porphyry copper deposits: Geology, v. 42, p. 1075–1078.
Pettke, T., Oberli, F., and Heinrich, C.A., 2010, The magma and metal source of giant porphyry-type ore deposits, based on lead isotope microanalysis of individual fluid inclusions: Earth and Planetary Scientific Letters, v. 296, p. 267–277.
Putnam, R., Glazner, A.F., Coleman, D.S., Kylander-Clark, A.R.C., Pavelsky, T., and Abbot, M.I., 2015, Plutonism in three dimensions: Field and geochemical relations on the southeast face of El Capitan, Yosemite National Park, California: Geosphere, v. 11, p. 1–25.
Ratajeski, K., Sisson, T.W., and Glazner, A.F., 2005, Experimental and geochemical evidence for derivation of the El Capitan Granite, California, by partial melting of hydrous gabbroic lower crust: Contributions to Mineralogy and Petrology, v. 149, p. 713–734.
Ricketts, J.W., Kelley, S.A., Karlstrom, K.E., Schmandt, B., Donahue, M.S., and van Wijk, J., 2016, Synchronous opening of the Rio Grande rift along its entire length at 25-10 Ma supported by apatite (U-Th)/He and fission-track thermochronology, and evaluation of possible driving mechanisms: Geological Society of America Bulletin, v. 128, p. 397–424.
Rosera, J.M., Coleman, D.S., and Stein, H.J., 2013, Re-evaluating genetic models for porphyry Mo mineralization at Questa New Mexico: Implications for ore deposition following silicic ignimbrite eruption: Geochemistry, Geophysics, Geosystems, v. 14, p. 787–805.
Rosera, J.M., Gaynor, S.P., and Coleman, D.S., 2021, Spatio-temporal shifts in magmatism and mineralization in northern Colorado beginning in the Late Eocene: Economic Geology, v. 116, p. 987–1010.
Rosera, J.M., Frazer, R.E., Mills, R.D., Jacob, K., Gaynor, S.P., Coleman, D.S., and Farmer, G.L., in press, Fluorine-rich mafic lower crust in the southern Rocky Mountains: The role of pre-enrichment in generating fluorine-rich silicic magmas and porphyry Mo deposits: American Mineralogist, https://doi.org/10.2138/am-2022-8503.
Ross, P.S., Jebrak, M., and Walker, B.M., 2002, Discharge of hydrothermal fluids from a magma chamber and concomitant formation of a stratified breccia zone at the Questa porphyry molybdenum deposit, New Mexico: Economic Geology, v. 97, p. 1679–1699.
Rowe, A., 2012, Ore genesis and fluid evolution of the Goat Hill orebody, Questa Climax-type porphyry-Mo system, NM, and its comparison to the Climax-type deposits of the Colorado Mineral Belt: Ph.D. thesis, Socorro, New Mexico Institute of Mining and Technology, 269 p.
Schilling, J.H., 1960, Mineral resources of Taos County, New Mexico: New Mexico State Bureau of Mines and Mineral Resources, Bulletin 71, 136 p.
Schöpa, A., Annen, C., Dilles, J.H., Sparks, R.S.J., and Blundy, J.D., 2017, Magma emplacement rates and porphyry copper deposits: Thermal modeling of the Yerington batholith, Nevada: Economic Geology, v. 112, p. 1653–1672.
Shannon, J.R., Walker, B.M., Carten, R.B., and Geraghty, E.P., 1982, Unidirectional solidification textures and their significance in determining relative ages of intrusions at the Henderson Mine, Colorado: Geology, v. 10, no. 6, p. 293–297.
Sillitoe, R.H., 1980, Cauldron subsidence a possible inhibitor of porphyry copper formation: Mining Geology Special Issue, v. 8, p. 85–93.
——2010, Porphyry copper systems: Economic Geology, v. 105, p. 3–41.
Sisson, T.W., Ratajeski, K., Hankins, W.B., and Glazner, A.F., 2005, Voluminous granitic magmas from common basaltic sources: Contributions to Mineralogy and Petrology, v. 148, p. 635–661.
Smith, G.A., Moore, J.D., and McIntosh, W.C., 2002, Assessing roles of volcanism and basin subsidence in causing Oligocene-Lower Miocene sedimentation in the Northern Rio Grande Rift, New Mexico, U.S.A.: Journal of Sedimentary Research, v. 72, p. 836–848.
Snelson, C., Keller, G.R., Miller, K.C., Rumpel, H.M., and Prodehl, C., 2005, Regional crustal structure derived from the CD-ROM 99 seismic refraction/wide-angle reflection profiles: The lower crust and upper mantle: America Geophysical Union, Geophysical Monograph Series, v. 154, p. 271–292.
Snyder, G.R., 1984, Paleomagnetism of the Questa mine area, Taos County, New Mexico: M.S. thesis, Golden, Colorado, Colorado School of Mines, 111 p.
Stein, H.J., 1985, A lead, strontium, and sulfur isotope study of the Laramide-Tertiary intrusions and mineralization in the Colorado mineral belt with emphasis on Climax-type porphyry molybdenum systems plus a summary of other newly acquired isotopic and rare earth element data: Ph.D. dissertation, Chapel Hill, North Carolina, University of North Carolina at Chapel Hill, 493 p.
Stein, H.J., and Crock, J.G., 1990, Late Cretaceous-Tertiary magmatism in the Colorado mineral belt; Rare earth element and samarium-neodymium isotopic studies: Geological Society of America, Memoir 74, p. 195–223.
Stein, H.J., and Hannah, J.L., 1985, Movement and origin of ore fluids in Climax-type systems: Geology, v. 13, p. 469–474.
Tappa, M.J., Coleman, D.S., Mills, R.D., and Samperton, K.M., 2011, The plutonic record of a silicic ignimbrite from the Latir volcanic field, New Mexico: Geochemistry, Geophysics, Geosystems, v. 12, 16 p.
Tapster, S., Condon, D.J., Naden, J., Noble, S.R., Petterson, M.G., Roberts, N.M.W., Saunders, A.D., and Smith, D.J., 2016, Rapid thermal rejuvenation of high-crystallinity magma linked to porphyry copper deposit formation; evidence from the Koloua Porphyry Prospect, Solomon Islands: Earth and Planetary Science Letters, v. 442, p. 206–217.
Tomlinson, D.H.J., Christiansen, E.H., Keith, J.D., Dorais, J.D., Ganske, R., Fernandez, D., Vetz, N., Sorensen, M., and Gibbs, J., 2021, Nature and origin of zoned polymetallic (Pb-Zn-Cu-Ag-Au) veins from the Bingham Canyon porphyry Cu-Au-Mo deposit, Utah: Economic Geology, v. 116, p. 747–771.
Thompson, P.M.E., Kempton, P.D., and Kerr, A.C., 2008, Evaluation of the effects of alteration and leaching on Sm-Nd and Lu-Hf systematics in submarine mafic rocks: Lithos, v. 104, p. 164–176.
Thompson, R.A., Dungan, M.A., and Lipman, P.W., 1986, Multiple differentiation processes in early-rift calc-alkaline volcanics, northern Rio Grande rift, New Mexico: Journal of Geophysical Research, v. 91, p. 6046–6058.
Zhao, Q., Zhai, D., Mathur, R., Liu, J., Selby, D., and Williams-Jones, A.E., 2021, The giant Chalukou porphyry Mo deposit, northeast China: The product of a short-lived, high flux mineralizing event: Economic Geology, v. 116, p. 1209–1225.
Zimmerer, M.J., and McIntosh, W.C., 2012, The geochronology of volcanic and plutonic rocks at the Questa caldera: Constraints on the origin of caldera-related silicic magmas: Geological Society of America Bulletin, v. 124, p. 1394–1408.
Zimmerman, A., Stein, H.J., Hannah, J.L., Koželj, D., Bogdanov, K., and Berza, T., 2008, Tectonic configuration of the Apuseni-Banat–Timok-Srednogorie belt, Balkans-South Carpathians, constrained by high precision Re-Os molybdenite ages: Mineralium Deposita, v. 43, p. 1–21.

Sean Gaynor is currently an associate professional specialist at Princeton University. He received a Ph.D. degree from University of North Carolina at Chapel Hill (2018), followed by a three-and-a-half-year postdoctoral study at the University of Geneva. His interests include large igneous provinces, batholith formation, supervolcano eruptions, igneous petrology, global climate change in deep time, economic geology, thermochronology, extensional tectonics, and the development of high-precision geochronology. During his Ph.D. studies, Sean also worked for two summers as a mine geologist at the Questa Mo mine in New Mexico.